respectively (Figures 3e and f). Taken together, these results suggested that YAP contributes to expression of a wide range of cell cycle-promoting genes and induces MM cell proliferation, although knockdown of individual YAP target genes shows moderate effects.

In conclusion, we showed that YAP induces multiple gene expression, which includes cell cycle-promoting genes such as *CCND1* and *FOXM1* in MM cells. Our findings thus serve to elucidate some important aspects of dysregulated cell cycle control mechanisms in MM cells through YAP activation. As individual inhibition of YAP target genes did not suppress MM proliferation sufficiently, we speculate that a wide range of genes evoked by YAP activation induce MM cell proliferation and progression as a whole. Thus, our results suggest that YAP itself may be a key target molecule for the development of a new molecular target therapy for MM.

CONFLICT OF INTEREST

The authors declare no conflict of interest.

ACKNOWLEDGEMENTS

We thank Ms Mika Yamamoto for her excellent technical assistance. This work was supported in part by a Special Coordination Fund for Promoting Science and Technology from the Ministry of Education, Culture, Sports, Science and Technology of Japan (H18-1-3-3-1), KAKENHI (18390245, 22300338), Grant-in-Aid for Third-Term Comprehensive Control Research for Cancer from the Ministry of Health, Labor and Welfare of Japan, the Takeda Science Foundation and the Kobayashi Foundation for Cancer Research.

REFERENCES

1 Pass HI, Vogelzang N, Hahn S, Carbone M. Malignant pleural mesothelioma. *Curr Probl Cancer* 2004; **28**: 93-174.
2 Yang H, Testa JR, Carbone M. Mesothelioma epidemiology, carcinogenesis, and pathogenesis. *Curr Treat Options Oncol* 2008; **9**: 147-157.
3 Robinson BW, Lake RA. Advances in malignant mesothelioma. *N Engl J Med* 2005; **353**: 1591-1603.
4 Vogelzang NJ, Rusthoven JJ, Symanowski J, Denham C, Kaukel E, Ruffie P *et al.* Phase III study of pemetrexed in combination with cisplatin versus cisplatin alone in patients with malignant pleural mesothelioma. *J Clin Oncol* 2003; **21**: 2636-2644.
5 Carbone M, Kratzke RA, Testa JR. The pathogenesis of mesothelioma. *Semin Oncol* 2002; **29**: 2-17.
6 Sekido Y. Genomic abnormalities and signal transduction dysregulation in malignant mesothelioma cells. *Cancer Sci* 2010; **101**: 1-6.
7 Illei PB, Ladanyi M, Rusch VW, Zakowski MF. The use of CDKN2A deletion as a diagnostic marker for malignant mesothelioma in body cavity effusions. *Cancer* 2003; **99**: 51-56.
8 Bianchi AB, Mitsunaga SI, Cheng JQ, Klein WM, Jhanwar SC, Seizinger B *et al.* High frequency of inactivating mutations in the neurofibromatosis type 2 gene (NF2) in primary malignant mesotheliomas. *Proc Natl Acad Sci USA* 1995; **92**: 10854-10858.
9 Sekido Y, Pass HI, Bader S, Mew DJ, Christman MF, Gazdar AF *et al.* Neurofibromatosis type 2 (NF2) gene is somatically mutated in mesothelioma but not in lung cancer. *Cancer Res* 1995; **55**: 1227-1231.
10 Bott M, Brevet M, Taylor BS, Shimizu S, Ito T, Wang L *et al.* The nuclear deubiquitinase BAP1 is commonly inactivated by somatic mutations and 3p21.1 losses in malignant pleural mesothelioma. *Nat Genet* 2011; **43**: 668-672.
11 Testa JR, Cheung M, Pei J, Below JE, Tan Y, Sementino E *et al.* Germline BAP1 mutations predispose to malignant mesothelioma. *Nat Genet* 2011; **43**: 1022-1025.
12 Hamaratoglu F, Willecke M, Kango-Singh M, Nolo R, Hyun E, Tao C *et al.* The tumour-suppressor genes NF2/Merlin and expanded act through Hippo signalling to regulate cell proliferation and apoptosis. *Nat Cell Biol* 2006; **8**: 27-36.
13 Dong J, Feldmann G, Huang J, Wu S, Zhang N, Comerford SA *et al.* Elucidation of a universal size-control mechanism in Drosophila and mammals. *Cell* 2007; **130**: 1120-1133.
14 Saucedo LJ, Edgar BA. Filling out the Hippo pathway. *Nat Rev Mol Cell Biol* 2007; **8**: 613-621.
15 Zhang N, Bai H, David KK, Dong J, Zheng Y, Cai J *et al.* The Merlin/NF2 tumor suppressor functions through the YAP oncoprotein to regulate tissue homeostasis in mammals. *Dev Cell* 2010; **19**: 27-38.
16 Murakami H, Mizuno T, Taniguchi T, Fujii M, Ishiguro F, Fukui T *et al.* LATS2 is a tumor suppressor gene of malignant mesothelioma. *Cancer Res* 2011; **71**: 873-883.
17 Yokoyama T, Osada H, Murakami H, Tatematsu Y, Taniguchi T, Kondo Y *et al.* YAP1 is involved in mesothelioma development and negatively regulated by Merlin through phosphorylation. *Carcinogenesis* 2008; **29**: 2139-2146.
18 Sekido Y. Inactivation of Merlin in malignant mesothelioma cells and the Hippo signaling cascade dysregulation. *Pathol Int* 2011; **61**: 331-344.
19 Huang J, Wu S, Barrera J, Matthews K, Pan D. The Hippo signaling pathway coordinately regulates cell proliferation and apoptosis by inactivating Yorkie, the Drosophila homolog of YAP. *Cell* 2005; **122**: 421-434.
20 Tapon N, Harvey KF, Bell DW, Wahrer DC, Schiripo TA, Haber DA *et al.* Salvador promotes both cell cycle exit and apoptosis in Drosophila and is mutated in human cancer cell lines. *Cell* 2002; **110**: 467-478.
21 Cao X, Pfaff SL, Gage FH. YAP regulates neural progenitor cell number via the TEA domain transcription factor. *Genes Dev* 2008; **22**: 3320-3334.
22 Nishioka N, Inoue K, Adachi K, Kiyonari H, Ota M, Ralston A *et al.* The Hippo signaling pathway components Lats and Yap pattern Tead4 activity to distinguish mouse trophectoderm from inner cell mass. *Dev Cell* 2009; **16**: 398-410.
23 Zhang X, Milton CC, Humbert PO, Harvey KF. Transcriptional output of the Salvador/Warts/Hippo pathway is controlled in distinct fashions in Drosophila melanogaster and mammalian cell lines. *Cancer Res* 2009; **69**: 6033-6041.
24 Zhao B, Ye X, Yu J, Li L, Li W, Li S *et al.* TEAD mediates YAP-dependent gene induction and growth control. *Genes Dev* 2008; **22**: 1962-1971.
25 Hall CA, Wang R, Miao J, Oliva E, Shen X, Wheeler T *et al.* Hippo pathway effector Yap is an ovarian cancer oncogene. *Cancer Res* 2010; **70**: 8517-8525.
26 Muramatsu T, Imoto I, Matsui T, Kozaki K, Haruki S, Sudol M *et al.* YAP is a candidate oncogene for esophageal squamous cell carcinoma. *Carcinogenesis* 2011; **32**: 389-398.
27 Wang Y, Dong Q, Zhang Q, Li Z, Wang E, Qiu X. Overexpression of yes-associated protein contributes to progression and poor prognosis of non-small-cell lung cancer. *Cancer Sci* 2010; **101**: 1279-1285.
28 Xu MZ, Yao TJ, Lee NP, Ng IO, Chan YT, Zender L *et al.* Yes-associated protein is an independent prognostic marker in hepatocellular carcinoma. *Cancer* 2009; **115**: 4576-4585.
29 Zhang X, George J, Deb S, Degoutin JL, Takano EA, Fox SB *et al.* The Hippo pathway transcriptional co-activator, YAP, is an ovarian cancer oncogene. *Oncogene* 2011; **30**: 2810-2822.
30 Basu S, Totty NF, Irwin MS, Sudol M, Downward J. Akt phosphorylates the Yes-associated protein, YAP, to induce interaction with 14-3-3 and attenuation of p73-mediated apoptosis. *Mol Cell* 2003; **11**: 11-23.
31 Lapi E, Di Agostino S, Donzelli S, Gal H, Domany E, Rechavi G *et al.* PML, YAP, and p73 are components of a proapoptotic autoregulatory feedback loop. *Mol Cell* 2008; **32**: 803-814.
32 Levy D, Adamovich Y, Reuven N, Shaul Y. The Yes-associated protein 1 stabilizes p73 by preventing Itch-mediated ubiquitination of p73. *Cell Death Differ* 2007; **14**: 743-751.
33 Anbanandam A, Albarado DC, Nguyen CT, Halder G, Gao X, Veeraraghavan S. Insights into transcription enhancer factor 1 (TEF-1) activity from the solution structure of the TEA domain. *Proc Natl Acad Sci USA* 2006; **103**: 17225-17230.
34 Vassilev A, Kaneko KJ, Shu H, Zhao Y, DePamphilis ML. TEAD/TEF transcription factors utilize the activation domain of YAP65, a Src/Yes-associated protein localized in the cytoplasm. *Genes Dev* 2001; **15**: 1229-1241.
35 Xiao GH, Gallagher R, Shetler J, Skele K, Altomare DA, Pestell RG *et al.* The NF2 tumor suppressor gene product, merlin, inhibits cell proliferation and cell cycle progression by repressing cyclin D1 expression. *Mol Cell Biol* 2005; **25**: 2384-2394.

Supplementary Information accompanies the paper on the Oncogene website (http://www.nature.com/onc)

Carcinogenesis vol.33 no.7 pp.1277–1285, 2012
doi:10.1093/carcin/bgs154
Advance Access publication April 24, 2012

Integrated analysis of genetic and epigenetic alterations reveals CpG island methylator phenotype associated with distinct clinical characters of lung adenocarcinoma

Keiko Shinjo[1,2], Yasuyuki Okamoto[1], Byonggu An[1], Toshihiko Yokoyama[3], Ichiro Takeuchi[4], Makiko Fujii[1], Hirotaka Osada[1,2], Noriyasu Usami[5], Yoshinori Hasegawa[3], Hidemi Ito[6], Toyoaki Hida[7], Nobukazu Fujimoto[8], Takumi Kishimoto[8], Yoshitaka Sekido[1,2] and Yutaka Kondo[1,9,*]

[1]Division of Molecular Oncology, Aichi Cancer Center Research Institute, 1-1 Kanokoden, Chikusa-ku, Nagoya 464-8681, Japan, [2]Department of Cancer Genetics, [3]Department of Respiratory Medicine, Nagoya University Graduate School of Medicine, Nagoya, Japan, [4]Graduate School of Engineering, Nagoya Institute of Technology, Nagoya, Japan, [5]Division of General Thoracic Surgery, Nagoya University Graduate School of Medicine, Nagoya, Japan, [6]Division of Epidemiology and Prevention, Aichi Cancer Center Research Institute, Nagoya, Japan, [7]Department of Thoracic Oncology, Aichi Cancer Center Hospital, Nagoya, Japan, [8]Department of Respiratory Medicine, Okayama Rosai Hospital, Okayama, Japan and [9]Precursory Research for Embryonic Science and Technology (PRESTO), Japan Science and Technology Agency, Saitama, Japan

*To whom correspondence should be addressed. Tel: +81 52 764 2994; Fax: +81 52 764 2994;
Email: ykondo@aichi-cc.jp

DNA methylation affects the aggressiveness of human malignancies. Cancers with CpG island methylator phenotype (CIMP), a distinct group with extensive DNA methylation, show characteristic features in several types of tumors. In this study, we initially defined the existence of CIMP in 41 lung adenocarcinomas (AdCas) through genome-wide DNA methylation microarray analysis. DNA methylation status of six CIMP markers newly identified by microarray analysis was further estimated in a total of 128 AdCas by bisulfite pyrosequencing analysis, which revealed that 10 (7.8%), 40 (31.3%) and 78 (60.9%) cases were classified as CIMP-high (CIMP-H), CIMP-low and CIMP-negative (CIMP-N), respectively. Notably, CIMP-H AdCas were strongly associated with wild-type epidermal growth factor receptor (*EGFR*), males and heavy smokers ($P = 0.0089$, $P = 0.0047$ and $P = 0.0036$, respectively). In addition, CIMP-H was significantly associated with worse prognosis; especially among male smokers, CIMP-H was an independent prognostic factor (hazard ratio 1.7617, 95% confidence interval 1.0030–2.9550, $P = 0.0489$). Compellingly, the existence of CIMP in AdCas was supported by the available public datasets, such as data from the Cancer Genome Atlas. Intriguingly, analysis of AdCa cell lines revealed that CIMP-positive AdCa cell lines were more sensitive to a DNA methylation inhibitor than CIMP-N ones regardless of *EGFR* mutation status. Our data demonstrate that CIMP in AdCas appears to be a unique subgroup that has distinct clinical traits from other AdCas. CIMP classification using our six-marker panel has implications for personalized medical strategies for lung cancer patients; in particular, DNA methylation inhibitor might be of therapeutic benefit to patients with CIMP-positive tumors.

Introduction

Lung cancer is the leading cause of human cancer death worldwide (1). Recent targeted therapies have improved the survival of patients with certain types of lung cancer, especially adenocarcinoma (AdCa), a common type of non-small cell lung cancer. AdCas with epidermal growth factor receptor (*EGFR*) mutation benefit particularly from EGFR tyrosine kinase inhibitors (TKIs) (2), whereas those harboring *EML4–ALK* fusion are highly sensitive to anaplastic lymphoma kinase (ALK) inhibitors (3). Despite these recent advances in targeted therapy for AdCas, a considerable number of patients with lung cancer still suffer from recurrence of disease. AdCas without such mutations are generally less sensitive to these targeted therapies than tumors with mutations. Given the evidence that the frequency of *EGFR* mutations account for up to 30% of AdCas, and even *EML4–ALK* fusions are found in AdCas albeit at a lower frequency, elucidating the underlying mechanisms other than such gene alterations in lung carcinogenesis is desirable to facilitate the development of new strategies for lung cancer treatment.

Studies have shown that in addition to genetic alterations, accumulation of epigenetic alterations play an important role in tumorigenesis of lung cancer (4). DNA methylation, an important epigenetic factor, affects the chromatin structure and is closely associated with gene regulation (5). Simultaneous dysregulation of multiple genes, including those involved in cell cycle, cell growth, cell death or cell adhesion, by DNA methylation may be a strong driving force to undergo transformation, sometimes in correlation with potentiated aggressiveness of the tumors (6).

Recent studies in colon cancer have shown that a subset of tumors suffer from a remarkably high rate of aberrant promoter DNA methylation at a large number of loci, referred to as CpG island methylator phenotype (CIMP) (7). CIMP tumors in colon exhibit distinct genetic and clinical features, such as high rates of *BRAF* and *KRAS* mutations, low frequency of *TP53* mutation, specific histology, proximal location and characteristic clinical outcome, suggesting that CIMP-related cancers may proceed through a unique pathway (8). In lung cancer, some studies have shown the existence of a subgroup of tumors with the characteristic methylation status of CIMP (9–13). However, in comparison with the considerable research of CIMP markers performed in colon cancers (7,14–16), no studies have assessed which DNA methylation markers can predict the most extensively methylated subgroups (i.e. CIMP) in lung AdCas due to the lack of accompanied genome-wide DNA methylation analysis in multiple samples. Since different panels of markers may lead to different classification of lung cancer (9,11), it is important to define markers that can accurately identify CIMP.

To examine whether CIMP exists as a characteristic subgroup in AdCas, we initially performed global screening for genes with aberrant DNA hypermethylation by the methylated CpG island amplification microarray (MCAM) analysis, which provides reproducible results with a high validation rate (16–20). Using the six CIMP markers newly identified by MCAM analysis, we characterized a distinct subgroup of AdCas exhibiting CIMP. In addition, several AdCa cell lines with different CIMP status were treated with a DNA methylation inhibitor, and the relationship between DNA methylation status and drug sensitivity was assessed. Our data provide evidence for a new strategy for lung cancer treatment.

Abbreviations: AdCa, adenocarcinoma; CIMP, CpG island methylator phenotype; CIMP-H, CIMP-high; CIMP-L, CIMP-low; CIMP-N, CIMP-negative; EGFR, epidermal growth factor receptor; MCAM, methylated CpG island amplification microarray; TCGA, the cancer genome atlas; TKI, tyrosine kinase inhibitor;

Materials and methods

Cell lines

A549 was purchased from the American Type Culture Collection (Rockville, MD) and PC9 was purchased from Immuno-Biological Laboratories (Fujioka, Gunma, Japan). NCI-H23, NCI-H358, NCI-H920, NCI-H2009, NCI-H1573, NCI-H1650 and HCC4011 were kind gifts from Dr Adi F. Gazdar (University of Texas Southwestern Medical Center, Dallas, TX) and Dr Mitsuo Sato (Nagoya University Graduate School of Medicine, Nagoya, Japan). Y-ML13 (ML13) and ACC-H1 (H1) were established in our institute. All cell lines were maintained in RPMI-1640 medium (Sigma–Aldrich, St Louis, MO) supplemented with 10%

fetal bovine serum (Invitrogen, Carlsbad, CA) and antibiotic–antimycotic reagent (Invitrogen) at 37°C in a humidified incubator with 5% CO_2.

5-Aza-dC treatment of cells

Cells were treated with 50 nM–1 μM 5-aza-2′-deoxycytidine (5-Aza-dC; Sigma–Aldrich) as described previously (17) or the TKI AG1478 (Calbiochem, San Diego, CA) for 72 h. DNA was extracted on the seventh day following treatment. Changes in proliferation were determined by using the TetraColor ONE (Seikagaku, Tokyo, Japan) system, containing 2-(2-methoxy-4-nitrophenyl)-3-(4-nitrophenyl)-5-(2,4-disulfophenyl)-2H-tetrazolium, monosodium salt and 1-methoxy-5-methylphenazinium methylsulfate as the electron carrier. After 1 h incubation at 37°C, absorbance was read at 450 nm with a multiplate reader. Growth inhibition was expressed as a mean ratio of absorbance reading from treated versus untreated cells. Cell numbers were also counted under a light microscope at the same time point.

Tissue samples

We collected 128 AdCa samples and 26 normal lung tissues from patients who underwent surgical resection at the Aichi Cancer Center Central Hospital, Okayama Rosai Hospital, Nagoya University Hospital and its affiliated hospitals in Japan, in accordance with the institutional policy. Samples and clinical data were collected after appropriate institutional review board approval was received and written informed consent had been obtained from all the patients. Histological and cytological examination of normal lung tissues, which were obtained from the lung cancer patients, revealed no remarkable findings as malignant tissues. In the normal tissues, no aberrant methylation was detected in 10 genes by pyrosequencing analysis (Supplementary Table 1, available at *Carcinogenesis* Online). A sample size of 124 patients was calculated to be sufficient to provide a survival rate difference of 25% with a significance level of 0.05 and power of 80%, when the frequency of CIMP-AdCa was estimated to be ~20% as is observed in colorectal cancer (8); therefore, we collected 128 AdCas to analyze the significance of CIMP (Table I).

DNA preparation

Genomic DNA was extracted using a standard phenol–chloroform method. Fully methylated DNA was prepared by treating genomic DNA with *SssI* methylase (New England Biolabs, Ipswich, MA), and unmethylated DNA was prepared by treating genomic DNA with phi29 DNA polymerase (GenomiPhi DNA Amplification Kit; Amersham Biosciences, Uppsala, Sweden) according to the manufacturers' protocol.

DNA methylation analysis

We performed bisulfite treatment as described previously (21,22).The DNA methylation levels were measured using pyrosequencing technology (Pyrosequencing AB, Uppsala, Sweden). Primer sequences and polymerase chain reaction conditions are shown in Supplementary Table 2, available at *Carcinogenesis* Online. All the primers were designed to examine the methylation status of CpGs within 0.5 kb of the transcription start site. A methylation level >15% was considered methylation positive since lower values could not be easily distinguished from background (17–20).

Methylated CpG island amplification microarray

For MCAM analysis, we randomly selected 41 cases from the 128 AdCas without any bias (average age was 61.9 years, ranging from 36 to 83 years old; Table I). A detailed protocol of MCA has been described previously (16–20). Briefly, amplicons from individual AdCas were labeled with Cy5 dye and cohybridized against amplicons from normal controls labeled with Cy3 dye on 15 K custom-promoter microarrays from Agilent Technologies (G4497A; Agilent Technologies, Santa Clara, CA) containing 6157 unique genes, which we had initially validated in a previous study (17). A Cy5/Cy3 signal in excess of 2.0 in MCAM was considered methylation positive (17–19). Comparison of the MCAM signal ratio (Cy5/Cy3 > 2.0 or Cy5/Cy5 ≤ 2.0) with the methylation status (positive or negative) from the pyrosequencing analysis showed a good concordance between the two analyses (sensitivity, 68.0% and specificity, 88.7%; Supplementary Table 3, available at *Carcinogenesis* Online).

Hierarchical clustering analysis

Cluster analysis was performed using an agglomerative hierarchical clustering algorithm (18,23). For specimen clustering, pairwise similarity measures among specimens were calculated using the Cluster 3.0 software (http://rana.lbl.gov/EisenSoftware.htm) or Minitab 15 statistical software (http://www.minitab.com), based on the DNA methylation intensity measurements

Table I. Clinical and molecular features according to the CIMP status

	All cases (%)	CIMP-N (%)	CIMP-L (%)	CIMP-H (%)	*P* value
Cases	128 (100)	78 (60.9)	40 (31.3)	10 (7.8)	
Age (mean ± SD)	64.7 ± 9.8	63.9 ± 10.0	66.4 ± 9.8	63.8 ± 7.0	0.4043
Gender					
Male	71 (55.5)	35 (44.9)	27 (67.5)	9 (90.0)	0.0047
Female	57 (44.5)	43 (55.1)	13 (32.5)	1 (10.0)	
Stage[a]					
I	75 (59.5)	51 (67.1)	21 (52.5)	3 (30.0)	0.2259
II	19 (15.1)	7 (9.2)	8 (20.0)	3 (30.0)	
III	29 (23.0)	16 (21.1)	10 (25.0)	4 (40.0)	
IV	3 (2.4)	2 (2.6)	1 (2.5)	0 (0)	
Smoking status					
Heavy smoker	41 (32.3)	21 (27.6)	12 (30.8)	8 (80.0)	0.0036
Light smoker	29 (22.8)	15 (19.7)	13 (33.3)	1 (10.0)	
Never-smoker	57 (44.9)	42 (55.3)	14 (35.9)	1 (10.0)	
Differentiation[a]					
Well	15 (17.4)	11 (21.2)	3 (10.7)	1 (16.7)	0.3552
Moderate	55 (64.0)	30 (57.6)	22 (78.6)	3 (50.0)	
Poorly	16 (18.6)	11 (21.2)	3 (10.7)	2 (33.3)	
Recurrence[a]					
(−)	41 (42.3)	27 (43.5)	14 (46.7)	0 (0)	0.1394
(+)	56 (57.7)	35 (56.5)	16 (53.3)	5 (100)	
EGFR mutation					
(−)	80 (62.5)	42 (53.8)	28 (70.0)	10 (100)	0.0089
(+)	48 (37.5)	36 (46.2)	12 (30.0)	0 (0)	
KRAS mutation					
(−)	118 (92.2)	74 (94.9)	36 (90.0)	8 (80.0)	0.2113
(+)	10 (7.8)	4 (5.1)	4 (10.0)	2 (20.0)	
p53 mutation[a]					
(−)	89 (69.5)	57 (74.0)	28 (73.7)	4 (40.0)	0.16
(+)	35 (27.3)	20 (26.0)	10 (26.3)	5 (50.0)	
BRAF mutation					
(−)	86 (100)	56 (100)	23 (100)	7 (100)	NA
(+)	0 (0)	0 (0)	0 (0)	0 (0)	

[a]Data were not available in some cases. Recurrence was observed within 5 years after surgery.

across all genes. *K*-means consensus clustering was performed with the R statistical package. A dendrogram and heat map were constructed using either TreeView (http://rana.lbl.gov/EisenSoftware.htm) or R statistical computing environment (http://cran.r-project.org).

Nearest neighbor classification

Using the DNA methylation status of six CIMP markers (positive or negative by pyrosequencing analysis), nearest neighbor classification was employed to classify the validation set consisting of 87 independent AdCas (24). In this analysis, each validation case was classified into one of the three clusters identified in the training set. The number of nearest neighbors was set as $k = 4$ because the smallest cluster (cluster 1) was consisted of four cases. The analysis was conducted using R statistical computing environment (http://cran.r-project.org).

Mutation analysis

Mutations in *KRAS* (codons 12 and 13) were analyzed by direct sequencing and the pyrosequencing method (25,26). *EGFR* mutations (exons 18–21) and *TP53* mutations (exons 5–8) were examined using direct sequencing (19,25). Mutation of *BRAF* (codon 600) was determined by the pyrosequencing method as previously reported (27). The polymerase chain reaction primer sequences used are listed in Supplementary Table 2, available at *Carcinogenesis* Online.

The Cancer Genome Atlas data

We obtained the methylation data of AdCa samples from the The Cancer Genome Atlas data (TCGA) web site (http://tcga-data.nci.nih.gov/tcga/tcgaHome2.jsp), and data of 85 AdCa samples (batches 34 and 37) were included in the analysis, which was conducted using the Illumina Infinium Human DNA Methylation 27 platform. The 3833 most variant probes from 27 578 CpG dinucleotides were used for further analysis, and a β value > 0.4 was considered as methylation positive.

Statistical analysis for clinical features

All statistical analyses were performed using the JMP statistical software version 5.1 (SAS Institute, Cary, NC). Fisher's exact test was used to determine non-random associations between two categorical variables. Kruskal–Wallis analysis was used to evaluate the extent of differences among more than three groups. All reported *P* values are two sided, with $P < 0.05$ taken as statistically significant. Patients were followed until incidence of death or until October 2010, whichever came first. Survival information was available for 118 of the 128 cases. Overall survival was calculated from the date of surgery until the date of death or the date the patient was last known to be alive (censored). The median follow-up time was 42.5 months. Overall survival curves were generated via the Kaplan–Meier method, and the log-rank test was used for statistical analysis. A multivariate analysis using the Cox proportional hazards model was performed to estimate the hazard ratio. All variables for the multivariate analysis were categorical variables (age, stage and CIMP status).

Results

Identification of a distinct subgroup with characteristic DNA methylation profiling in AdCas

First, we evaluated the genome-wide DNA methylation status in a training set of 41 AdCas using MCAM analysis (18–20). Among 6157 genes on the microarray, we selected 1156 genes that are commonly methylated across >10% of AdCas and performed consensus average linkage hierarchical clustering analysis (28). In terms of DNA methylation, AdCas could be divided into three clusters, with clustering stability increasing for $k = 2$ to $k = 3$ but not for more than $k = 3$ (Figure 1A, Supplementary Figure 1, available at *Carcinogenesis* Online). Intriguingly, all four cases in cluster 1 stably fell into the same cluster regardless of *k* values (2–5), whereas 12 cases (92%) and 24 cases (96%) fell into clusters 2 and 3, respectively, indicating a high similarity of their methylation profile among each of the three-cluster member. The number of DNA methylated genes showed bimodal distribution in AdCas; DNA methylation was highly accumulated in two AdCas, both of which fell into cluster 1# (Figure 1B). Consistently, a majority of the genes were commonly methylated across more than half of the AdCas in cluster 1, whereas common methylation targets were detected in ≤50% of the AdCas in clusters 2 and 3 ($P < 0.001$, Figure 1C). In addition, the average number of methylated genes was 766.8 ± 70.4, 485.7 ± 40.6 and 319.2 ± 28.1 in clusters 1, 2 and 3 (k=3), respectively ($P < 0.001$) (Figure 1D). These observations indicated that extensively methylated AdCas exist, which appear to be characterized by correlated CpG island DNA methylation of a subset of genes in a subset of tumors, whereas AdCas with less extensive DNA methylation or with rare DNA methylation were classified into discrete subgroups (7,14–16).

Identification of CIMP markers in AdCas

MCAM analysis suggested the existence of a distinct subgroup with extensive DNA methylation in AdCas. Because CIMP status is closely associated with clinical outcome in forming a distinct subgroup in colon cancer, glioma and breast cancer (29–31), it is useful to accurately identify CIMP tumors without performing microarray analysis, which may reveal the etiology and clinical correlates of CIMP in AdCas. First, we examined whether the DNA methylation status of the classical CIMP markers (*p16*, *MINT1*, *MINT2*, *MINT31* and *MLH1*), which are effective for diagnosis of CIMP in colon cancer (32), reflected the methylation profile, especially CIMP, determined by MCAM analysis in AdCas (Figure 2A, left panel). CIMP-positive AdCas defined by the classical CIMP markers were not consistent with all the extensively methylated AdCas in cluster 1, suggesting that these markers are not always accurate for diagnosis of the extensively methylated AdCas.

To establish a new panel of a minimum number of CIMP markers without reducing the classification power, which was readily applied to a large number of tumor samples, we eliminated the genes from the target genes of methylation in MCAM analysis (Figure 2B). The initial definition of CIMP was based on concordant methylation of Type C loci (cancer-specific methylation) (7). Therefore, we first excluded markers that showed evidence of DNA methylation in normal tissues, which means Type A loci (age-related methylation) (7). Then, we selected 232 genes that were methylated in >75% of AdCas in cluster 1 but were methylated in <30% in the other clusters. Among these genes, 10 genes fulfilled the criteria of (i) concomitant array signals in all the probes for the same genes on the microarray, (ii) methylation-positive probes were located within 500 bp from transcription start sites and (iii) enable to design the stable and reproducible pyrosequencing assay using the candidate genes. Finally, we selected six candidate markers, *CCNA1*, *ACAN*, *GFRA1*, *EDARADD*, *MGC45800* and *p16* (*CDKN2A*), to determine CIMP in AdCas using a statistical model based on recursive descent partition analysis with the pyrosequencing data of 10 genes (33).

DNA methylation status of this panel of six markers was examined in 41 AdCas using pyrosequencing analysis. These six markers were frequently methylated in four (10%) AdCas of cluster 1, which showed DNA methylation in five or more of the six markers (Figure 2A, right panel). We designated this subgroup as CIMP-high (CIMP-H). In contrast, 26 (63%) AdCas were rarely methylated; none or one marker was methylated in this subgroup. The majority of AdCas (21 cases, 81%) in this subgroup fell into cluster 3, which showed the lowest frequency of DNA methylation. We defined AdCas with methylation in none or only one of the six markers as CIMP-negative (CIMP-N). The intermediate subgroup (11 cases, 27%) between CIMP-H and CIMP-N showed DNA methylation in two to four markers of the six selected CIMP markers. We designated this subgroup as CIMP-low (CIMP-L), in which 7 (64%) of 11 AdCas fell into cluster 2 and showed intermediate frequency of DNA methylation.

Validation analysis of newly identified CIMP markers

It is important to note that this initial selection of the six candidate markers did not introduce a bias for detecting CIMP only in the training set. Therefore, the newly identified panel of six markers was independently confirmed in a validation set of 87 AdCas. Among them, we found 6 (7%) CIMP-H, 30 (34%) CIMP-L and 51 (59%) CIMP-N tumors, which were of a similar frequency as observed in the training set of 41 AdCas (Supplementary Figure 2, available at *Carcinogenesis* Online). To estimate whether the classification by the six CIMP markers in the validation set was compatible with the CIMP classification in the training set, we performed the nearest four neighborhood prediction analysis (Figure 2C, see Materials and Methods). This

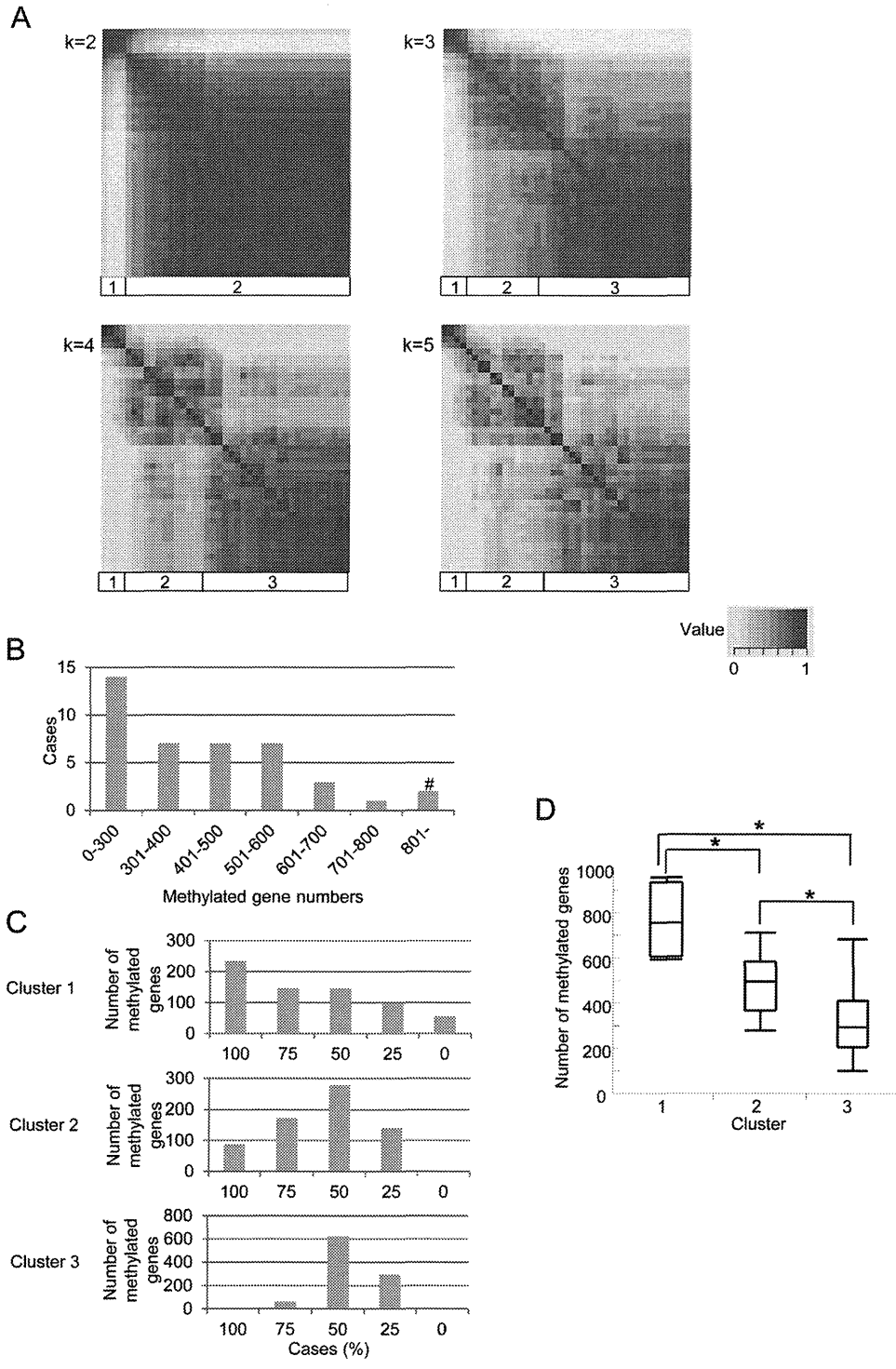

Fig. 1. DNA methylation profiling by MCAM analysis. (**A**) Consensus clustering analysis was performed with the 1156 genes from the AdCa cases for $k = 2, 3, 4$ and 5. The samples are listed in the same order on the x- and y-axes. Clusters are designated as are indicated at the bottom of each panel. Consensus index values range from 0 (highly dissimilar) to 1 (highly similar). (**B**) The distribution of number of methylated genes. X-axis indicates the number of methylated genes. Y-axis indicates cases. Two AdCas were highly methylated (#). (**C**) Distribution of number of methylated genes in each cluster. In total of 679 genes, in which methylation was observed in 20–80% of 41 AdCas, were analyzed. (**D**) Box and whisker plots of the number of methylated genes in each cluster. The mean is marked by a horizontal line inside the box whose ends denote the upper and lower quartiles. Error bars represent 5th and 95th percentile values, $^*P < 0.001$.

analysis defined 6 of 87 AdCas in the validation set as cluster 1, all of which were also categorized as CIMP-H tumors according to our criteria using the six-marker panel. Furthermore, 51 AdCas that were classified as cluster 3 with a probability >80% by the nearest neighbor classification analysis were also classified as CIMP-N tumors by our six CIMP marker panel. These results indicate that the three clusters are highly reproducible, and our panel of six markers is capable of accurately categorizing cases into these three clusters.

Identification of AdCa–CIMP in the Cancer Genome Atlas data set

Next, we examined whether the six CIMP markers could also be applicable in classifying AdCas deposited in TCGA (http://tcga-

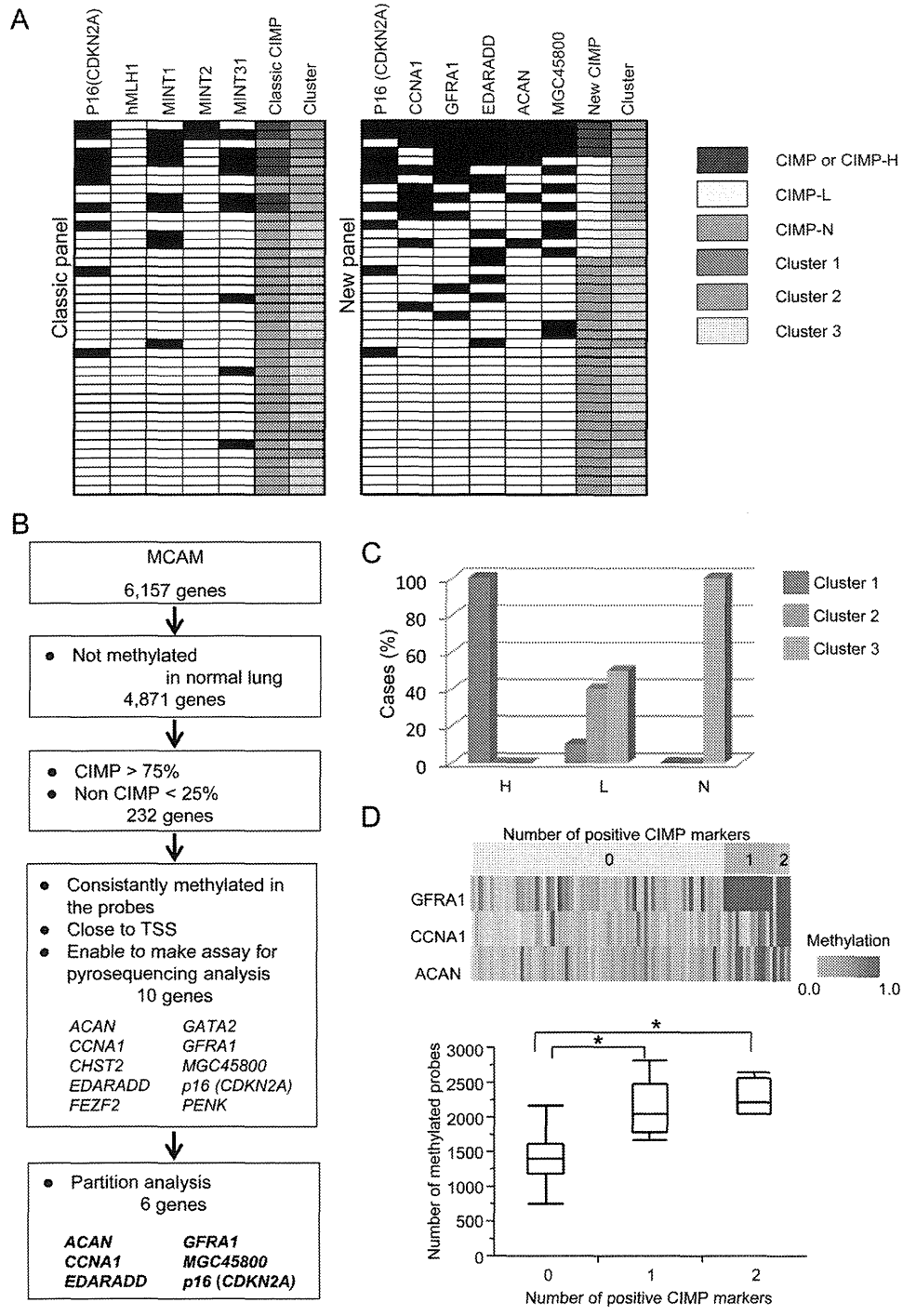

Fig. 2. DNA methylation profiling in AdCa using pyrosequencing analysis. (**A**) Comparison of classification by CIMP markers with the clusters determined by consensus clustering analysis (Figure 1A). Left: tumors with methylation in at least two of the five classical CIMP markers were determined as CIMP. Right: a panel of new CIMP markers classified CIMP-H (five or six of six markers), CIMP-L (two to four of six markers) and CIMP-N (zero or one of six markers), respectively. Black, methylation positive and white boxes, methylation negative. Clusters 1, 2 and 3 correspond to clusters 1, 2 and 3 in Figure 1A. The samples are listed in the same order on the *y*-axis in both panel. (**B**) Schema of selection for a new panel of six CIMP markers. TSS, transcription start site. (**C**) Nearest neighbor classification analysis in the validation set. Relationship between CIMP status determined by six CIMP markers, and the cluster determined by consensus cluster analysis are shown. H, CIMP-H; L, CIMP-L and N, CIMP-N. Clusters 1, 2 and 3 correspond to clusters 1, 2 and 3 in Figure 1A. (**D**) Analysis of DNA methylation status of three CIMP markers, GFRA1, CCNA1 and ACAN using the data set (3833 probes) from the Cancer Genome Atlas data set. Upper panel, heat map overview of three genes in 85 AdCas. Color corresponds to the methylation level as indicated; red is high (β value = 1.0) and yellow is low (β value = 0.0) levels of DNA methylation. Lower panel: relationship between number of methylated probes (β value > 0.4) among 3833 probes and the number of methylated genes of CIMP markers. $^{*}P < 0.001$.

data.nci.nih.gov/tcga/tcgaHome2.jsp) (30). DNA methylation data of 85 AdCas were obtained from the TCGA database, which were analyzed by the Infinium BeadChip containing 27 578 probes corresponding to 14 473 genes. Among those probes, we found that some probes corresponding to three of our new CIMP markers (*ACAN*, *CCNA1* and *GFRA1*) were located close to the regions where we conducted the pyrosequencing analysis. In contrast, no probes corresponding to the other three CIMP markers (*CDKN2A*,

MGC45800 and *EDARADD*) were located within 500 bp of transcription start sites, which was a condition of our pyrosequencing analysis. Therefore, we examined the classification power of the three CIMP markers (*ACAN*, *CCNA1* and *GFRA1*) in the 85 AdCas obtained from the TCGA. None, 4 (4.7%), 14 (16.5%) and 67 (78.8%) AdCas showed DNA methylation in three, two, one or none of the three CIMP markers, respectively (DNA methylation positive, β value > 0.4, Figure 2D, upper panel). AdCas with DNA methylation in one or two CIMP markers had more methylated probes among the 3833 most variant probes than those who had no methylation in the CIMP markers (average methylated probes: 1430.8 ± 39.5, 2116.4 ± 86.3 and 2288.8 ± 161.5, in AdCas with none, one or two methylated CIMP markers, respectively, $P < 0.001$; Figure 2D, lower panel). These data suggested that the methylation status of the three CIMP markers is also predictive for highly methylated AdCas in the TCGA data set.

Clinical significance of CIMP tumors in lung AdCa

Next, we assessed whether CIMP-positive AdCas form a distinct subgroup with characteristic clinical features. We combined two sets of AdCa cohorts (training set and validation set) for the analysis of CIMP signatures, with a total of 128 cases. We did not access any clinical information before CIMP classification of both sets of AdCas to avoid any bias in the analysis of the clinical significance of CIMP tumors. Of the 128 pooled AdCas, 10 (7.8%) were classified as CIMP-H, 40 (31.3%) as CIMP-L and 78 (60.9%) as CIMP-N (Figure 3A). CIMP-H tumors were more prevalent in males ($P = 0.0047$) and associated with frequent exposure to smoking (pack year > 40, $P = 0.0036$). Intriguingly, we found a tight association between CIMP and *EGFR* status ($P = 0.0089$; Table I). None of the 10 CIMP-H AdCas contained any *EGFR* mutations, whereas 36/78 (46.2%) CIMP-N and 12/40 (30.0%) CIMP-L AdCas had *EGFR* mutations. In contrast, no such tendency was observed between CIMP status and *KRAS*, *TP53* and *BRAF* mutations.

To investigate whether CIMP status had any impact on overall survival, we performed Kaplan–Meier survival analysis and found that CIMP-H was a significantly negative prognostic factor ($P = 0.0115$, log-rank test; Figure 3B). Since *EGFR* mutations have been indicated as a potential positive prognostic factor for survival in advanced non-small cell lung cancer patients treated with chemotherapy with or without TKI (34), we analyzed overall survival according to the *EGFR* mutation status. Among the AdCas harboring wild-type *EGFR*, CIMP-H tumors still correlated with poor survival ($P = 0.0312$, log-rank test; Figure 3C). In addition to a worse prognosis in patients with AdCas who were smokers ($P = 0.0373$, log-rank test; Figure 3D), we found that CIMP-H was an independent prognostic factor among male smokers (hazard ratio 1.7617, 95% confidence interval 1.0030–2.9550, $P = 0.0489$; Figure 3E). Taken together, these findings indicated that CIMP-H tumors have unique clinical features that distinguish them from the other AdCas.

Clinical implication of epigenetic therapy for lung AdCa

To evaluate the relationship between CIMP status and effects of the DNA methylation inhibitor, 5-Aza-dC, as an antitumor agent, we first analyzed DNA methylation status of the six CIMP markers in 14 AdCa cell lines, including one CIMP-H (H358), seven CIMP-L (H23, H1, PC9, H2009, H3255, H1975 and H1650) and six CIMP-N cell lines (H920, A549, HCC827, ML13, H1573 and HCC4011) (Supplementary Table 4, available at *Carcinogenesis* Online). CIMP-H cells (H358) harbor wild-type *EGFR*, whereas the CIMP-L and CIMP-N cells harbor either wild-type (H23, H1, H2009, H1975, H920, A549, HCC827, ML13 and H1573) or mutated (PC9, H3255, H1650 and HCC4011) *EGFR*. Regardless of the CIMP status, cells with wild-type *EGFR* showed resistance to the TKI, AG1478 (Figure 4A). Intriguingly, antitumor activity of 5-Aza-dC appeared to be associated with CIMP status. Each cell line showed different IC50, which were significantly lower in the CIMP-positive cells (average, CIMP-H and CIMP-L) than in the CIMP-N cells ($P = 0.02$, average IC50 was 68, 229 and 982 nM, respectively, Figure 4B). To determine a more accurate relationship between DNA demethylation and antitumor activity, we used level of *LINE-1* demethylation, which represents the global level of methylation, as a surrogate marker of 5-Aza-dC treatment. We examined the power of growth inhibition at a concentration of ~20% of *LINE-1* demethylation. Cell growth of CIMP-H and CIMP-L cells was significantly inhibited at each concentration of 5-Aza-dC, in contrast to CIMP-N cells, the majority of which did not respond to the treatment (Figure 4B). These data suggest that in addition to CIMP-H AdCas, tumorigenesis of CIMP-L AdCas may also depend on DNA methylation silencing pathway to some extent.

Discussion

In the current study, we performed a comprehensive genome-wide DNA methylation analysis and identified a distinct molecular subgroup (CIMP-H) in human AdCas. This subgroup showed a remarkably high rate of DNA methylation in correlated cancer-specific CpG island hypermethylation of a subset of genes, indicating the existence of CIMP in AdCas (7).

Previously, studies suggested the existence of CIMP in lung cancer. The first study defined a CIMP-positive case as having a tumor with aberrant methylation in either *CDH13* or *CRBP1* and found that CIMP-positive cases showed poorer prognosis than the CIMP-N ones (9). Although a consistent clinical feature, poor prognosis of CIMP-positive cases, was observed between our study and the previous ones, frequencies of CIMP and the other clinicopathological features associated with CIMP were varied, probably due to the different panels of CIMP marker examined (9,11–13). Thus, it is still unclear which DNA methylation markers can define the most extensively methylated subgroups (CIMP) due to the lack of accompanied genome-wide analysis in the previous AdCa studies. If CIMP affects only a subset of CpG islands in a subgroup of AdCas, collection of data for a large numbers of markers from numerous tumor samples is required to identify CIMP in AdCas. Indeed, we found in the current study that CIMP-positive tumors diagnosed by the original CIMP markers defined in the colon cancer study (7) were not consistent with the extensively methylated AdCas, suggesting that these markers are not always applicable for diagnosis of CIMP tumors other than colon cancers. Thus, the existence of CIMP in AdCas from the global point of view has remained elusive before the current study. Our genome-wide MCAM analysis successfully identified six practical and representative markers for the prediction of CIMP in AdCas.

Integrated analysis of the DNA methylation status of the six CIMP markers with several cancer-associated gene mutations, including *EGFR*, *TP53*, *KRAS* and *BRAF*, revealed that CIMP-H tumors in both the training and the validation sets did not harbor any *EGFR* mutations, suggesting that the two events are mutually exclusive, whereas mutations in the other three genes did not show such strong associations with CIMP status. Thus, our six novel markers enabled us to decipher the negative association between CIMP and *EGFR* mutations, which had been only suggested by previous studies (35). Indeed, CIMP-H tumors are significantly associated with males, frequent exposure to smoking and high relapse rate of disease, which clearly differ from the typical features of *EGFR*-mutant AdCas, such as association with females, non-habit forming smoking and better prognosis. Interestingly, colorectal cancers also show strong association between CIMP status and smoking (36,37). Thus, smoking may be one of the potential causes of CIMP. These data suggested that a particular set of genes are methylated in CIMP-H AdCas, and their target genes are involved in activation of an alternative pathway, in which tumorigenesis may be minimally dependent on *EGFR* mutation.

The association of better clinical outcome with CIMP-positive tumors has been reported in breast cancer, colon cancer and glioma. Fang *et al.* (31) showed that there was significant overlap of CIMP targets in those different types of cancers. Among the 33 overlapped CIMP targets between the cancers, we found that the DNA methylation status of 19 genes was available from our MCAM analysis. Using

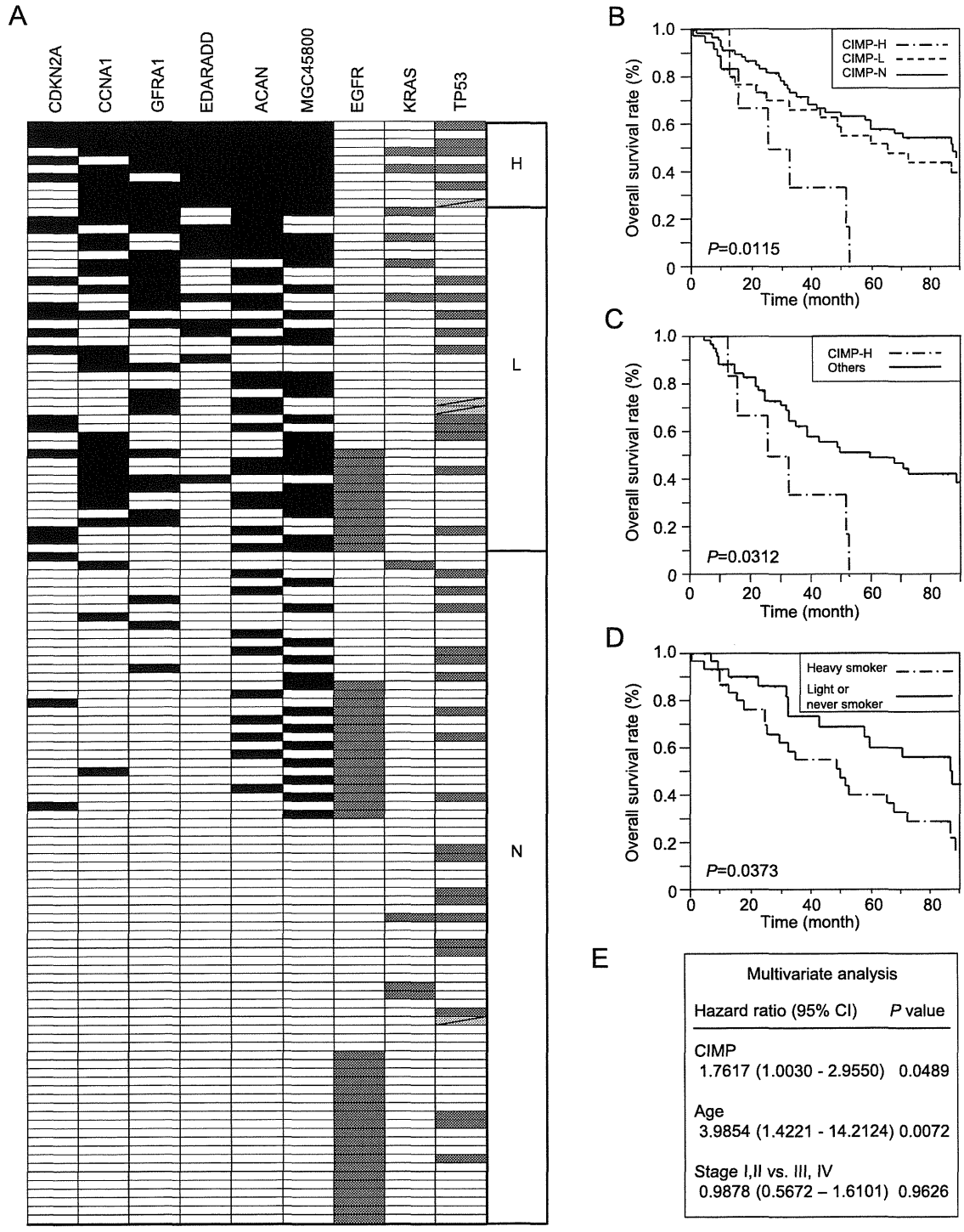

Fig. 3. CIMP status associated with prognosis of AdCas. (**A**) Total of 128 AdCas were classified into three subclasses by the six newly identified CIMP markers. Black boxes, methylation positive; gray boxes, mutation positive; white boxes, methylation negative or mutation negative and light gray boxes with oblique lines, data were not available for *TP53* status. H, CIMP-H; L, CIMP-L and N, CIMP-N. (**B**) Kaplan–Meier analysis for overall survival of 128 AdCa patients by CIMP status. *P* value was calculated by log-rank analysis. (**C**) Kaplan–Meier analysis for overall survival of 80 AdCas cases harboring wild-type *EGFR* by CIMP status. (**D**) Kaplan–Meier analysis for overall survival by smoking status. (**E**) Multivariate analysis showed that CIMP-H was an independent prognostic factor among male smokers (n = 37).

the methylation status of these 19 genes, we found that AdCas in our training set were divided into three clusters; the three most extensively methylated AdCas were consistent with the CIMP-H AdCas, suggesting that a panel of 19 genes may also be a potent predictor for CIMP-H in AdCas (Supplementary Figure 3, available at *Carcinogenesis* Online). However, given the worse prognosis of patients with CIMP-H AdCas, the impact of CIMP to survival in lung cancer might be different from the CIMP in colon cancer, glioma and breast cancer. Indeed, a study in myelodysplastic syndromes also showed that the presence of CIMP was significantly associated with poor prognosis and risk of leukemia transformation (38). The contrasting impacts of CIMP to clinical outcome might be due to the distinct DNA methylation profiles specific to each tumor type; CIMP confers poor prognosis in lung AdCas and myelodysplastic syndromes via inactivation

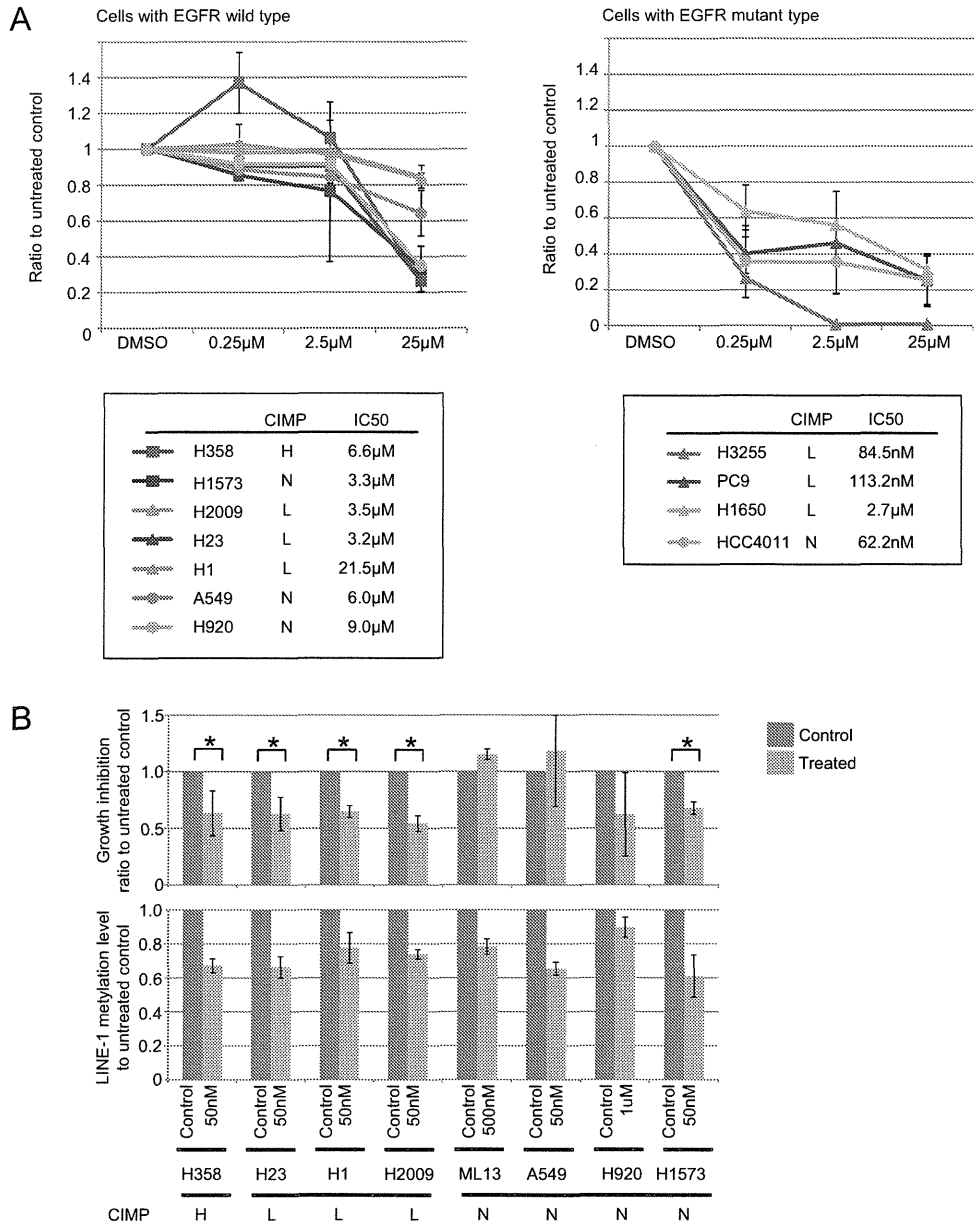

Fig. 4. Epigenetic treatment in AdCa cell lines. (**A**) Growth rate of AdCa cell lines with each *EGFR* status as measured by 3-(4,5-dimethylthiazole-2-yl)-2,5-bdiphenyl tetrazolium bromide assay after 72 h of treatment of TKI (AG1478) in different doses. CIMP status of each cell line is indicated by H, L and N. (**B**) Growth inhibition of AdCas after 5-Aza-dC treatment. Growth inhibition was examined (upper panel) at the concentration where 20% of LINE-1 demethylation had occurred (lower panel). $^{*}P < 0.05$.

of genes critical for tumor progression and for response to chemotherapy.

We found another epigenomic subgroup (CIMP-L) of AdCas within the major subclasses classified by DNA methylation status. This subtype showed moderate accumulation of DNA methylation. Indeed, our cell line study showed that CIMP-L cells were sensitive to 5-Aza-dC treatment. These data suggest that tumorigenesis pathway of CIMP-L AdCas might also be affected by DNA methylation to a certain extent. However, we could not find any specific features of this subtype. This might be due to the lack of suitable markers to further classify CIMP-L, resulting in a mixture of subpopulations as was found in the colon cancer study (39,40). Sensitive and specific markers for CIMP-L in AdCas are needed to further characterize CIMP-L. Additional studies will be required to address this problem.

CIMP-positive lung AdCa cell lines appeared to be more sensitive to 5-Aza-dC treatment, in which demethylation effectively occurred even at low doses of 5-Aza-dC, regardless of *EGFR* mutation status. Epigenetic drugs targeting DNA methylation, such as 5-Aza-dC and 5-azacytidine, have shown clinical effectiveness in cancer treatment, especially for hematological malignancies (41,42). For the treatment of thoracic malignancies, studies showed that a certain population of patients with AdCas clinically benefit from 5-Aza-dC treatment (43,44). One of the important issues of research is the identification of biomarkers predictive of response to DNA methylation inhibitors (45). Our cell line analysis showed that CIMP status appeared to be associated with response to 5-Aza-dC, suggesting that epigenetic therapy might be a useful approach, especially for those individuals who have been diagnosed with CIMP. If this possibility was validated, our findings would be significant for the use of DNA methylation inhibitors in lung tumors.

In conclusion, we demonstrated here that six newly identified CIMP markers may be useful in the accurate and practical epigenomic

classifications of lung cancer. Our findings may enable the development of new molecular diagnostics tools for personalized medicine for lung cancers and confer a new paradigm for cancer treatment.

Supplementary material

Supplementary Figures 1–3 and Tables 1–4 can be found at http://carcin.oxfordjournals.org/.

Funding

This work is supported by grants-in-aid for Cancer Research from the Ministry of Health. Labor and Welfare (to Y.K.) and a grant from the Japan Society for the Promotion of Science (to Y.K.).

Conflict of Interest Statement: None declared.

References

1. Jemal,A. *et al.* (2010) Cancer statistics, 2010. *CA Cancer J. Clin.*, **60**, 277–300.
2. Mitsudomi,T. *et al.* (2010) Gefitinib versus cisplatin plus docetaxel in patients with non-small-cell lung cancer harbouring mutations of the epidermal growth factor receptor (WJTOG3405): an open label, randomised phase 3 trial. *Lancet Oncol.*, **11**, 121–128.
3. Choi,Y.L. *et al.* (2010) EML4-ALK mutations in lung cancer that confer resistance to ALK inhibitors. *N. Engl. J. Med.*, **363**, 1734–1739.
4. Belinsky,S.A. (2004) Gene-promoter hypermethylation as a biomarker in lung cancer. *Nat. Rev. Cancer*, **4**, 707–717.
5. Jones,P.A. *et al.* (2002) The fundamental role of epigenetic events in cancer. *Nat. Rev. Genet.*, **3**, 415–428.
6. Jones,P.A. *et al.* (2007) The epigenomics of cancer. *Cell*, **128**, 683–692.
7. Toyota,M. *et al.* (1999) CpG island methylator phenotype in colorectal cancer. *Proc. Natl Acad. Sci. USA*, **96**, 8681–8686.
8. Grady,W.M. (2007) CIMP and colon cancer gets more complicated. *Gut*, **56**, 1498–1500.
9. Suzuki,M. *et al.* (2006) Exclusive mutation in epidermal growth factor receptor gene, HER-2, and KRAS, and synchronous methylation of non-small cell lung cancer. *Cancer*, **106**, 2200–2207.
10. Marsit,C.J. *et al.* (2006) Examination of a CpG island methylator phenotype and implications of methylation profiles in solid tumors. *Cancer Res.*, **66**, 10621–10629.
11. Liu,Z. *et al.* (2008) CpG island methylator phenotype involving tumor suppressor genes located on chromosome 3p in non-small cell lung cancer. *Lung Cancer*, **62**, 15–22.
12. Suzuki,M. *et al.* (2010) Molecular characterization of chronic obstructive pulmonary disease-related non-small cell lung cancer through aberrant methylation and alterations of EGFR signaling. *Ann. Surg. Oncol.*, **17**, 878–888.
13. Zhang,Y. *et al.* (2011) Methylation of multiple genes as a candidate biomarker in non-small cell lung cancer. *Cancer Lett.*, **303**, 21–28.
14. Weisenberger,D.J. *et al.* (2006) CpG island methylator phenotype underlies sporadic microsatellite instability and is tightly associated with BRAF mutation in colorectal cancer. *Nat. Genet.*, **38**, 787–793.
15. Ogino,S. *et al.* (2006) CpG island methylator phenotype-low (CIMP-low) in colorectal cancer: possible associations with male sex and KRAS mutations. *J. Mol. Diagn.*, **8**, 582–588.
16. Shen,L. *et al.* (2007) Integrated genetic and epigenetic analysis identifies three different subclasses of colon cancer. *Proc. Natl Acad. Sci. USA*, **104**, 18654–18659.
17. Gao,W. *et al.* (2008) Variable DNA methylation patterns associated with progression of disease in hepatocellular carcinomas. *Carcinogenesis*, **29**, 1901–1910.
18. Goto,Y. *et al.* (2009) Epigenetic profiles distinguish malignant pleural mesothelioma from lung adenocarcinoma. *Cancer Res.*, **69**, 9073–9082.
19. An,B. *et al.* (2010) A characteristic methylation profile in CpG island methylator phenotype-negative distal colorectal cancers. *Int. J. Cancer*, **127**, 2095–2105.
20. Okamoto,Y. *et al.* (2012) Aberrant DNA methylation associated with aggressiveness of gastrointestinal stromal tumour. *Gut*, **61**, 392–401.
21. Yang,A.S. *et al.* (2004) A simple method for estimating global DNA methylation using bisulfite PCR of repetitive DNA elements. *Nucleic Acids Res.*, **32**, e38.
22. Kondo,Y. *et al.* (2007) Alterations of DNA methylation and histone modifications contribute to gene silencing in hepatocellular carcinomas. *Hepatol Res.*, **37**, 974–983.
23. Eisen,M.B. *et al.* (1998) Cluster analysis and display of genome-wide expression patterns. *Proc. Natl Acad. Sci. USA*, **95**, 14863–14868.
24. Cover,T. *et al.* (1967) Nearest neighbor pattern classification. *IEEE Trans. Inform. Theory*, **13**, 21–27.
25. Yokoyama,T. *et al.* (2006) EGFR point mutation in non-small cell lung cancer is occasionally accompanied by a second mutation or amplification. *Cancer Sci.*, **97**, 753–759.
26. Ogino,S. *et al.* (2005) Sensitive sequencing method for KRAS mutation detection by pyrosequencing. *J. Mol. Diagn.*, **7**, 413–421.
27. Spittle,C. *et al.* (2007) Application of a BRAF pyrosequencing assay for mutation detection and copy number analysis in malignant melanoma. *J. Mol. Diagn.*, **9**, 464–471.
28. Monti,S. *et al.* (2003) Consensus clustering: a resampling-based method for class discovery and visualization of gene expression microarray data. *Mach. Learn.*, **52**, 91–118.
29. Toyota,M. *et al.* (2000) Distinct genetic profiles in colorectal tumors with or without the CpG island methylator phenotype. *Proc. Natl Acad. Sci. USA*, **97**, 710–715.
30. Noushmehr,H. *et al.* (2010) Identification of a CpG island methylator phenotype that defines a distinct subgroup of glioma. *Cancer Cell*, **17**, 510–522.
31. Fang,F. *et al.* (2011) Breast cancer methylomes establish an epigenomic foundation for metastasis. *Sci. Transl. Med.*, **3**, 75ra25.
32. Issa,J.P. (2004) CpG island methylator phenotype in cancer. *Nat. Rev. Cancer*, **4**, 988–993.
33. Lu,K.H. *et al.* (2004) Selection of potential markers for epithelial ovarian cancer with gene expression arrays and recursive descent partition analysis. *Clin. Cancer Res.*, **10**, 3291–3300.
34. Eberhard,D.A. *et al.* (2005) Mutations in the epidermal growth factor receptor and in KRAS are predictive and prognostic indicators in patients with non-small-cell lung cancer treated with chemotherapy alone and in combination with erlotinib. *J. Clin. Oncol.*, **23**, 5900–5909.
35. Toyooka,S. *et al.* (2006) Mutational and epigenetic evidence for independent pathways for lung adenocarcinomas arising in smokers and never smokers. *Cancer Res.*, **66**, 1371–1375.
36. Samowitz,W.S. *et al.* (2006) Association of smoking, CpG island methylator phenotype, and V600E BRAF mutations in colon cancer. *J. Natl Cancer Inst.*, **98**, 1731–1738.
37. Limsui,D. *et al.* (2010) Cigarette smoking and colorectal cancer risk by molecularly defined subtypes. *J. Natl Cancer Inst.*, **102**, 1012–1022.
38. Shen,L. *et al.* (2010) DNA methylation predicts survival and response to therapy in patients with myelodysplastic syndromes. *J. Clin. Oncol.*, **28**, 605–613.
39. Ogino,S. *et al.* (2008) Molecular classification and correlates in colorectal cancer. *J. Mol. Diagn.*, **10**, 13–27.
40. Yagi,K. *et al.* (2010) Three DNA methylation epigenotypes in human colorectal cancer. *Clin. Cancer Res.*, **16**, 21–33.
41. Silverman,L.R. *et al.* (2002) Randomized controlled trial of azacitidine in patients with the myelodysplastic syndrome: a study of the cancer and leukemia group B. *J. Clin. Oncol.*, **20**, 2429–2440.
42. Kantarjian,H. *et al.* (2006) Decitabine improves patient outcomes in myelodysplastic syndromes: results of a phase III randomized study. *Cancer*, **106**, 1794–1803.
43. Schrump,D.S. *et al.* (2006) Phase I study of decitabine-mediated gene expression in patients with cancers involving the lungs, esophagus, or pleura. *Clin. Cancer Res.*, **12**, 5777–5785.
44. Momparler,R.L. *et al.* (2001) Potential of 5-aza-2'-deoxycytidine (Decitabine) a potent inhibitor of DNA methylation for therapy of advanced non-small cell lung cancer. *Lung Cancer*, **34** (suppl. 4), S111–S115.
45. Garcia-Manero,G. (2010) Prognosis of myelodysplastic syndromes. *Hematology Am. Soc. Hematol. Educ. Program*, **2010**, 330–337.

Received November 20, 2011; revised April 9, 2012; accepted April 18, 2012

THE JOURNAL OF BIOLOGICAL CHEMISTRY VOL. 287, NO. 33, pp. 27396–27406, August 10, 2012

Contribution of MicroRNA-1275 to Claudin11 Protein Suppression via a Polycomb-mediated Silencing Mechanism in Human Glioma Stem-like Cells*[S]

Received for publication, March 5, 2012, and in revised form, June 18, 2012 Published, JBC Papers in Press, June 26, 2012, DOI 10.1074/jbc.M112.359109

Keisuke Katsushima[‡], Keiko Shinjo[‡§], Atsushi Natsume[¶], Fumiharu Ohka[‡], Makiko Fujii[‡], Hirotaka Osada[‡§], Yoshitaka Sekido[‡§], and Yutaka Kondo[‡‖1]

From the [‡]Division of Molecular Oncology, Aichi Cancer Center Research Institute, Nagoya 464-8681, Japan, [§]Department of Cancer Genetics, Nagoya Graduate School of Medicine, Nagoya 466-8560, Japan, and [¶]Department of Neurosurgery, Nagoya University School of Medicine, Nagoya 464-8560, Japan and the [‖]Precursory Research for Embryonic Science and Technology (PRESTO), Japan Science and Technology Agency (JST), Tokyo 102-0076, Japan

Background: Molecular mechanisms underlying heterogeneity of glioblastoma are poorly understood.
Results: Newly identified microRNA-1275, which is controlled by a polycomb-mediated silencing mechanism, regulates expression of oligodendroglial lineage protein, Claudin11, in glioma stem-like cells.
Conclusion: MicroRNA-1275 may contribute to the establishment of tissue heterogeneity via epigenetic mechanisms.
Significance: We identified a microRNA that is associated with tumor cell differentiation in the oligodendroglial lineage.

Glioblastomas show heterogeneous histological features, and tumor cells show distinct phenotypic states that confer different functional attributes and an aggressive character. However, the molecular mechanisms underlying the heterogeneity in this disease are poorly understood. Glioma stem-like cells (GSCs) are considered able to aberrantly differentiate into diverse cell types and may contribute to the establishment of tumor heterogeneity. Using a GSC model, we investigated differentially expressed microRNAs (miRNAs) and associated epigenetic mechanisms that regulate the differentiation of GSCs. miRNA profiling using microarray technology showed that 13 and 34 miRNAs were commonly up-regulated and down-regulated in two independent GSC lines during differentiation, respectively. Among this set of miRNAs, quantitative PCR analysis showed that miRNA-1275 (miR-1275) was consistently down-regulated during GSC differentiation, along with the up-regulation of its target, CLDN11, an important protein during oligodendroglial lineage differentiation. Inhibition of miR-1275 with a specific antisense oligonucleotide (anti-miR-1275) in GSCs increased the expression of CLDN11, together with significant growth suppression. Epigenetic analysis revealed that gain of histone H3 lysine 27 trimethylation (H3K27me3) in the primary microRNA-1275 promoter was closely associated with miR-1275 expression. Treatment with 3-deazaneplanocin A, an inhibitor of H3K27 methyltransferase, attenuated CLDN11 induction by serum stimulation in parallel with sustained miR-1275 expression. Our results have illuminated the epigenetic regulatory pathways of miR-1275 that are closely associated with oligodendroglial differentiation, which may contribute to the tissue heterogeneity seen in the formation of glioblastomas. Given that inhibition of miR-1275 induces expression of oligodendroglial lineage proteins and suppresses tumor cell proliferation, this may be a potential therapeutic target for glioblastomas.

Glioblastoma is the most common and deadly primary brain tumor, which is characterized by intratumoral and intertumoral heterogeneity with histologically different types of cells (1). Such multiple distinct subpopulations of cancer cells within tumors link to the existence of cells that survive surgery and chemotherapy to form recurrent lesions that are resistant to further treatments. Cumulative effort aimed at developing targeted therapies for glioblastomas has been somewhat hampered by complexities arising from tissue heterogeneity (2). Therefore, elucidating the molecular mechanisms underlying tissue heterogeneity of glioblastoma is a fundamental requirement for the development of effective treatments for this dreadful disease.

Evidence from several groups has shown that glioblastoma contain a rare, highly tumorigenic, self-renewing subpopulation of cells, called glioma stem-like cells (GSCs)[2] (3, 4). According to recent studies in a breast cancer model, cancer stem-like cells were able to aberrantly differentiate into diverse cell types by signals within the tumor microenvironments; such phenotypic plasticity between stem-like cells and differentiated nonstem-like cells may contribute to the establishment of tumor heterogeneity (5, 6). Indeed, the presence of such a cancer stem-like cell subpopulation has been shown in NOD-SCID mouse models to recapitulate the observed heterogeneity of

* This work was supported by a grant from PRESTO of JST (to Y. K.) and a grant-in-aid for scientific research from the Japan Society for the Promotion of Science (to Y. K.).
[S] This article contains supplemental Figs. 1–6 and Tables 1–3.
[1] To whom correspondence should be addressed: Division of Molecular Oncology Aichi Cancer Center Research Institute 1-1 Kanokoden, Chikusa-ku, Nagoya 464-8681, Japan. Tel. and Fax: 81-52-764-2994; E-mail: ykondo@aichi-cc.jp.

[2] The abbreviations used are: GSC, glioma stem-like cell; NSC, neural stem cell; miRNA, microRNA; miR, microRNA; pri-miR-1275, primary miR-1275; pre-miR-1275, precursor miR-1275; CLDN11, Claudin11; PRC, polycomb repressor complex; DZNep, 3-deazaneplanocin A; GFAP glial fibrillary acidic protein; MAP2, microtubule-associated protein 2; OLIG2, oligodendrocyte lineage transcription factor 2; KD, knockdown; S-BTC, serum-induced brain tumor cell; qPCR, quantitative PCR.

different types of human tumors (7–9). Thus, GSCs might be a good model for studying tumor cell differentiation and associated tissue heterogeneity.

microRNAs (miRNAs) are known to down-regulate the expression of genes by targeting 3′-untranslated regions (3′-UTRs) of mRNAs via direct mRNA degradation or translational inhibition (10). Studies have shown that miRNAs are potential key regulators of cellular differentiation and proliferation, which have been implicated in many types of cancers (11, 12). The roles of miRNAs in glioblastoma have also been studied. miR-9/9* is highly abundant in CD133+ cells, and inhibition of miR-9/9* leads to reduced neurosphere formation (13). miR-21 and miR-17–92 cluster were highly expressed in glioblastoma and appear to function in an anti-apoptotic role (14, 15). miR-221 and miR-222 were also up-regulated in glioblastoma and shown to be involved in cell cycle regulation via down-regulation of *CDKN1B* (16). Although the oncogenic or tumor-suppressive roles of these miRNAs in glioblastoma cells have been studied, the regulation of subtype-specific genes by miRNAs in tumor cells, especially in respect to differentiation of GSCs as linked to the establishment of tissue heterogeneity, has not been well studied.

Besides known genetic alterations, aberrant epigenetic alterations have emerged as common hallmarks of many cancers including glioblastoma (17–19). Epigenetic mechanisms can also regulate the expression of miRNAs (20, 21). Emerging data suggest a role for epigenetic controls in regulating tumor cell plasticity, where they can generate multiple distinct cellular subpopulations, thereby contributing to intratumoral heterogeneity (22). Histone H3 lysine 27 trimethylation (H3K27me3), which is catalyzed by polycomb repressor complex 2 (PRC2) and recognized by PRC1, is regarded as an easily reversible modification (23, 24). Recent data imply that PRC could act not only to maintain stemness and determine the proper lineage in pluripotent stem cells, but also to guide their further developmental processes by proper regulation of subtype-specific genes in progenitor cells (25).

Here, we investigated the molecular effects of the newly identified miR-1275 in GSC differentiation, whose expression is regulated via a PRC2-H3K27me3-dependent epigenetic mechanism in response to environmental cues, and assessed the relationship between stem-like cell differentiation and tissue heterogeneity, especially the oligodendroglial component in glioblastomas. Our results suggest that this developmental microRNA is regulated via an epigenetic pathway that contributes to the phenotypic diversity of glioblastoma tissues, which may in turn provide a better understanding of the heterogeneity of glioblastoma in the context of human neurodevelopment.

EXPERIMENTAL PROCEDURES

Cell Cultures—Glioblastoma tissue samples were obtained from patients undergoing surgical treatment at Nagoya University Hospital, Japan, after they provided written informed consent. The procedures used for derivation of GSCs (1228-GSC, 316-GSC, and 222-GSC) were described previously (26, 27). Briefly, dissociated tumor cells were cultured in neurobasal medium comprising Neurobasal media, with N2 and B27 supplements (Invitrogen), along with human recombinant basic fibroblast growth factor (bFGF) and epidermal growth factor (EGF) (20 ng/ml each; R&D Systems, Minneapolis, MN). Serum-induced brain tumor cells (S-BTCs) were established by culturing GSCs in DMEM (Invitrogen) containing 10% fetal bovine serum (FBS). T98, MDA231, MCF7, SKBR3, and PC3 cell lines were grown in DMEM with 10% FBS. A human neural stem cell (NSC) line was generated from the human fetal telencephalon as described previously (28). This human NSC line is capable of self-renewal and can differentiate into cells of neuronal and glial lineages, both *in vivo* and *in vitro*. NSCs were cultured in DMEM containing 0.1 mM 2-mercaptoethanol. After 2 days, NSCs were transferred to DMEM containing 0.5 μM retinoic acid (Sigma-Aldrich) and incubated for two additional days to induce differentiation. For the inhibition of PRC2 activity, GSCs were plated in dishes for 24 h before 3-deazaneplanocin A (DZNep) treatment (5 μM). GSCs were treated with DZNep or PBS (control) for 2–7 days. For the generation of stable knockdown of *EZH2* in GSC (*EZH2*-KD GSC), retroviral vectors were used as reported previously (29).

miRNA Microarray—Human miRNA Microarray V3 kits (G4470C; Agilent Technologies, Santa Clara, California) were used according to the manufacturer's protocols. This microarray system contains probes for all 866 human and 89 human viral miRNAs reported from the Sanger database v12.0 (miRBase). Each miRNA species is printed 20 times with replicate probes on the array. Total RNA was isolated from GSCs (1228, 316) and corresponding S-BTCs (continuous serum exposure for 21 days) with TRIzol reagent (Invitrogen). One hundred ng of total RNA was labeled with pCp-Cy3 (Agilent Technologies) and 15 units of T4 RNA ligase (GE Healthcare, Little Chalfont, Buckinghamshire, UK) at 16 °C for 2 h. Labeled samples were purified with Micro Bio-Spin 6 columns (Bio-Rad) and hybridized to microarrays at 55 °C with rotation at 20 rpm for 20 h. Microarrays were scanned by an Agilent Scanner (Agilent Scan Control 7.0 software) and analyzed using Agilent Feature Extraction 10.7 software for miRNA microarray profiling. Raw data were normalized and analyzed with the use of GeneSpring software (version 11.5; Silicon Genetics, Redwood City, CA). The data of our microarray are available in the ArrayExpress database with accession code: GSE36201. To analyze the target genes of differentially expressed miRNAs, we performed computational analysis using two miRNA target databases, namely TargetScan and the microRNA Search software from the Memorial Sloan-Kettering Cancer Center.

Quantitative Reverse Transcription-Polymerase Chain Reaction Analyses—One μg of RNA was reverse-transcribed with SuperScript III reverse transcriptase (Invitrogen). TaqMan PCR and SYBR Green quantitative PCR (qPCR) were carried out for the target genes in duplicate. TaqMan PCR assays (Applied Biosystems) and oligonucleotide primers used were as follows: miR-1275 (AB Assay ID 002840); miR-205 (AB Assay ID 000509); *RNU6B* (AB Assay ID 001093); *GAPDH* (AB Assay ID Hs00266705_g1); *EZH2* (AB Assay ID Hs00544830_m1); glial fibrillary acidic protein (*GFAP*) (AB Assay ID Hs00157674_m1); neuron-specific class III β-tubulin (*Tuj1*) (AB Assay ID Hs00964962_g1); Claudin11 (*CLDN11*), sense, 5′-CTGGTGGACATCCTCATCCT-3′, and antisense, 5′-CCAGCAGAATGAGCAAAACA-3′.

RT-PCR—To evaluate the transcript of pri-mir-1275, RT-PCR was performed using primers 1F, 5′-CTCTGTGAGAAAGGGTGTGG-3′ and 1R, 5′-TCTGCCTTGGGGAAAATAAG-3′; 2F, 5′-GCAGAAATACCTCACCAAGTTTTTA-3′ and 2R, 5′-TTTGGCATACTTACAGACACAAGAC-3′; 3F, 5′-CTCTGAAGTCTCTGGGTATTGCTCT-3′ and 3R, 5′-CACTCCATGTCTCTCCAGCTC-3′; and 4F, 5′-TGATCCTTATGTGGTAGTTTTAGGG-3′ and 4R, 5′-CAAAGAGTAATTGGAAGGAGAAGC-3′. Strand-specific reverse transcription was performed by SuperScript III first-strand synthesis system (Invitrogen) according to the manufacturer's instructions using 50 ng of total RNA or genomic DNA with strand-specific primers (1R, 2R, 3R, or 4R). Synthesized cDNA was amplified using FastStart *Taq* DNA polymerase (Roche Applied Science).

Western Blot Analysis—To perform Western blot analysis, the primary antibodies used were anti-CLDN11 (ab53041, Abcam; Cambridge, UK), anti-PAX5 (ab15164, Abcam), anti-NEUROD2 (ab109406, Abcam), and anti-β-actin (4967, Cell Signaling Technology, Danvers, MA) rabbit polyclonal antibodies. The secondary antibody used was HRP-linked anti-rabbit IgG antibody (7074, Cell Signaling Technology).

Manipulation of miR-1275 in Cell Lines—To examine the effects of miR-1275 (accession number, NR_031681), cells were transfected with the precursor molecules mimicking miR-1275 (pre-miR-1275 precursor, final concentration of 30 or 100 nM, Applied Biosystems) or negative control miRNA (pre-miR negative control 1, 30 or 100 nM, Applied Biosystems) according to the manufacturer's instructions. Inhibition of miR-1275 was performed using an anti-miR-1275 inhibitor (anti-miR-1275 inhibitor, 30 or 100 nM, Applied Biosystems) or a negative control anti-RNA (anti-miR inhibitor negative control 1, 30 or 100 nM, Applied Biosystems) according to the manufacturer's instructions.

Dual-Luciferase Reporter Assay—Two fragments of the *CLDN11* 3′-UTR region (1,381 bp and 431 bp to give pmir-CLDN11-3′-UTR and CLDN11 1/2) were prepared for luciferase constructs, which contain one or two potential target sites of miR-1275 (+1772 to +2202 and +822 to +2202 relative to the transcription start site, respectively (accession number, NR_031681); see supplemental Fig. 2). The fragments were amplified by PCR with the following primers: for pmir-CLDN11-3′-UTR, sense, 5′-GCTCGCTAGCCTCGAGTATAAGAGGGCT-3′, and antisense, 5′-GCAGGTCGACTCTAGATACCTCTGGATACAAC-3′; and for CLDN11 1/2, sense, 5′-GCCTCGAGAACCATGGTTTTCCTGAAAT-3′, and antisense, 5′-ACTCTAGATACCTCTGGATACAACAGAAGATT-3′. miRNA target site mutants were generated with the QuikChange site-directed mutagenesis kit (Stratagene, La Jolla, CA) using the following primers: Mut-1F, 5′-AACTTCTCCCCATTTCTTTTGGTTGCCT-3′, and Mut-1R, 5′-AGGCAACCAAAAGAAATGGGGAGAAGTT-3′; and Mut-2F, 5′-CACATTTTTAAAGCTTCTTTTCTCTCTATTTG-3′, and Mut-2R 5′-CAAATAGAGAGAAAAGAAGCTTTAAAAATGTG-3′, and sequence was verified. These primers produced *CLDN11* 3′-UTR fragments with deletion of seed sequences (5′-UCCCCCA-3′). The fragments of pmir-CLDN11-3′-UTR and CLDN11 1/2 were then ligated into the XbaI site of the pmirGLO luciferase reporter vector (Promega, Madison, WI). For the reporter assay, luciferase constructs (500 ng) were transfected into the cells using Lipofectamine 2000 (Invitrogen) with 30 or 100 nM miR-1275 (see above). Luciferase activity was measured 72 h after transfection using a Dual-Luciferase reporter assay system (Promega). To obtain the relative luciferase activity, firefly luminescence was normalized by the *Renilla* luminescence.

Cell Growth Assay—GSCs (5×10^3) were plated in 96-well culture dishes for 24 h before transfection of the anti-miR-1275 inhibitor, siRNAs against *CLDN11* (100 nM; siRNA 1, s9925 or siRNA 2, s9926, Applied Biosystems), or negative control (100 nM, AM4611, Applied Biosystems). The number of viable cells was counted on days 3 and 7 after transfection. Experiments were performed independently in triplicate.

Chromatin Immunoprecipitation (ChIP)—ChIP assays were performed based on a modification of previously published methods (30). Briefly, cells (1×10^6) were treated with 1% formaldehyde for 8 min to cross-link histones to DNA. After sonication of cell pellets, the lysate was incubated with 10 μl of anti-histone H3 (Abcam, ab1791), anti-K9 acetylated histone H3 (Abcam, ab6002), anti-K27 trimethylated histone H3 (Abcam, ab6002), or anti-YY1 antibodies (sc-281; Santa Cruz Biotechnology, Santa Cruz, CA). To collect the immunoprecipitated complexes, protein G-Sepharose beads (GE Healthcare) were added and incubated for 1 h at 4 °C. DNA was extracted by the phenol/chloroform method, ethanol-precipitated, and resuspended in water. ChIP products were assayed by SYBR Green ChIP-qPCR using the following sets of primers: sense, 5′-GTGACCTGCGGCTACACC-3′, and antisense, 5′-AGGATGAGGATGTCCACCAG-3′ encompassing *CLDN11* promoter region; sense, 5′-GCAGAAATACCTCACCAAGTTTTTA-3′, and antisense, 5′-TTTGGCATACTTACAGACACAAGAC-3′ encompassing the pri-miR-1275 promoter region.

Immunohistochemistry—Paraffin-embedded sections were immunostained with anti-CLDN11 antibody (sc-25711, Santa Cruz Biotechnology), anti-MAP2 antibody (ab11267, Abcam), anti-GFAP antibody (Z0334; DAKO, Glostrup, Denmark), or anti-OLIG2 antibody (MABN50, Millipore). Primary antibody-antigen complexes were visualized using horseradish peroxidase-conjugated secondary antibodies followed by diaminobenzidine or anti-mouse Alexa Fluor 546 and anti-rabbit Alexa Fluor 488 secondary antibodies (Molecular Probes, Eugene, OR). Nuclei were counterstained using 4′, 6-diamidino-2-phenylindole (DAPI).

Bisulfite Pyrosequencing Methylation Analysis—DNA was treated with sodium bisulfite as reported previously (31). Briefly, 2 μg of genomic DNA was denatured with 2 M NaOH for 10 min followed by incubation with 3 M sodium bisulfite (Sigma, pH 5.0) for 16 h at 50 °C. After treatment, DNA was purified via a Wizard miniprep column (Promega) and resuspended in 30 μl of diluted water. *CLDN11* promoter methylation was examined using pyrosequencing technology (Pyrosequencing AB, Uppsala, Sweden) as was reported previously (31). The primer sets used were as follows: sense, 5′-GAGAGGGTTATAAGAAGAGAAATTAG-3′, and antisense, 5′-GGGACACCGCTGATCGTTTAAATAACCCCAAAAAAA-

CCATTAA-3′; universal biotinylated primer, 5′-GGGACA-CCGCTGATCGTTTA-3′; and sequencing primer, 5′-TGG-AATTGTTTTATTTTGTA-3′.

Statistics—The statistical significance of the differences observed was determined by paired Student's *t* test or one-way analysis of variance (StadView software version 5.0; Abacus Concepts, Berkeley, CA). All reported *p* values were two-sided, with $p < 0.05$ considered statistically significant.

RESULTS

miRNA Expression Profiling during GSC Differentiation and Target Prediction—Glioblastoma spheroid cultures, which are enriched with GSCs, converted into differentiated adherent cells in response to serum within 48 h and were termed S-BTCs along with contributing to an attenuation of tumorigenicity in NOD-SCID mice as was reported previously (4, 26). To investigate the miRNAs involved in GSC differentiation, we examined miRNA expression before and after exposure to differentiation-promoting serum condition in two GSC models (316- and 1228-GSCs) using miRNA expression microarrays. Among the 866 human miRNAs on the microarray, 32 and 43 miRNAs were up-regulated, and 128 and 56 miRNAs were down-regulated with a greater than 2-fold difference before and after serum exposure in 1228-GSCs and 316-GSCs, respectively (supplemental Tables S1 and S2). Among these differentially expressed miRNAs, 13 and 34 miRNAs were commonly up-regulated and down-regulated in both 1228-GSCs and 316-GSCs, respectively (Fig. 1*A*).

We computationally analyzed the list of target genes of these differentially expressed miRNAs in two GSC lines using two independent publicly available database-related software programs, TargetScan and the microRNA Search software, because each program uses its own unique algorithms to measure complimentarily. Among the list of miRNAs and their targets, we focused on the miRNAs for which relevant targets are closely associated with neural cell differentiation. A profound relationship was found between miR-1275 and *CLDN11* (also known as oligodendrocyte-specific protein, *OSP*), a tight junction protein that is a major and essential component of central nervous system myelin and has been shown to increase in expression when oligodendrocyte progenitors develop into mature oligodendrocytes (32). Predicted target genes of miR-1275 that were commonly identified within two databases are listed in supplemental Table 3. miR-1275 appeared to have a strong target bias for the 3′-UTR mRNA of *CLDN11*; it has two predictive seed sequences in this 3′-UTR (Fig. 1*B*). Consistent with the microarray analysis, quantitative RT-PCR showed that the expression of miR-1275 was down-regulated during GSC differentiation, together with up-regulation of *CLDN11* in three independent GSC lines (1228-, 316-, and 222-GSCs; Fig. 1, *C* and *D*). Expression of the other significant miR-1275 targets, such as *GATA2B*, *CEBPG*, *PAX5*, and *NEUROD2* that are listed in the database and were validated by qPCR or Western blot analysis, did not appear to be significantly concordant with miR-1275 expression in our model, although *PAX5* and *NEUROD2* are associated with neural differentiation (33, 34) (supplemental Fig. 1, *A* and *B*). We also analyzed the expression levels of miR-205 in GSCs, which has been reported as a potential regulator of *CLDN11* in human embryonic stem cell differentiation (35), and found that miR-205 expression was at an extremely low level, and there was no evidence of dynamic alteration in response to serum in GSCs (supplemental Fig. 1*C*). Intriguingly, an inverse correlation between miR-1275 and *CLDN11* expression was also found in the NSCs. miR-1275 expression was down-regulated during the differentiation of NSCs induced by retinoic acid, together with *CLDN11* up-regulation (supplemental Fig. 1*D*).

Interaction between miR-1275 and Its Binding Sites in the CLDN11 3′-UTR—Because miRNAs negatively regulate mRNA expression by repressing translation or directly cleaving the targeted mRNA via imperfect binding to their 3′-UTR, we experimentally assessed the interaction between miR-1275 and the 3′-UTR of the *CLDN11* mRNA. First, we examined the levels of miR-1275 expression in five cancer cell lines, namely glioma cell line (T98), three breast cancer cell lines (MDA-MB-231, MCF7, and SKBR3), and a prostate cancer cell line (PC3), and in NSC by quantitative RT-PCR analysis. Low level of miR-1275 expression was observed in T98, whereas all the breast cancer cell lines and the prostate cancer cell line, as well as NSCs, showed moderate to high levels of miR-1275 expression (Fig. 2*A*).

To investigate the potential relationship between *CLDN11* 3′-UTR and miR-1275, the *CLDN11* 3′-UTR, which contained two predictive miR-1275 target sites, was cloned just downstream of the firefly luciferase coding sequence (pmir-CLDN11-3′-UTR) and transfected into the MDA231, MCF7, SKBR3, PC3, and T98 cell lines. Significant repression of luciferase activities was observed in the MDA-MB-231, MCF7, SKBR3, and PC3 cell lines, which expressed a high level of miR-1275, as compared with the control luciferase activity (Fig. 2*B*). On the other hand, no obvious changes of luciferase activity were observed in the T98 line, which expressed a substantially lower level of miR-1275.

Next, to further examine the direct interaction of miR-1275 with the potential target sites in the *CLDN11* 3′-UTR, we co-transfected the pmir-CLDN11-3′-UTR together with expression plasmids for miR-1275 into T98 cells. Significant repression of luciferase activities was observed under the miR-1275 expression condition (Fig. 2*C*). However, although it is statistically significant, the effect of robust miR-1275 up-regulation (more than 600 times higher than untransfected cells) in T98 cells transfected with pre-miR-1275 resulted in relatively small changes (decreases of around 30–40%) in *CLDN11*3′-UTR luciferase activity. In contrast, *CLDN11* 3′-UTR luciferase activity was prominently down-regulated in MDA231, MCF7, SKBR3, and PC3 cells as compared with T98 cells, although the difference in miR-1275 expression between these two groups was less than 10 times (Fig. 2, *A* and *B*). These data suggest the existence of another mechanism, such as other types of microRNAs in addition to miR-1275, that is involved in the regulation of *CLDN11* expression in T98 cells.

Conversely, repression of luciferase activities in PC3 was impaired by down-regulation of miR-1275 with a specific miR-1275 inhibitor (anti-miR-1275, 100 nM) (supplemental Fig. 2*A*). In addition, pmir-CLDN11-3′-UTR constructs with one or two mutated miR-1275 binding sites showed stepwise increase in

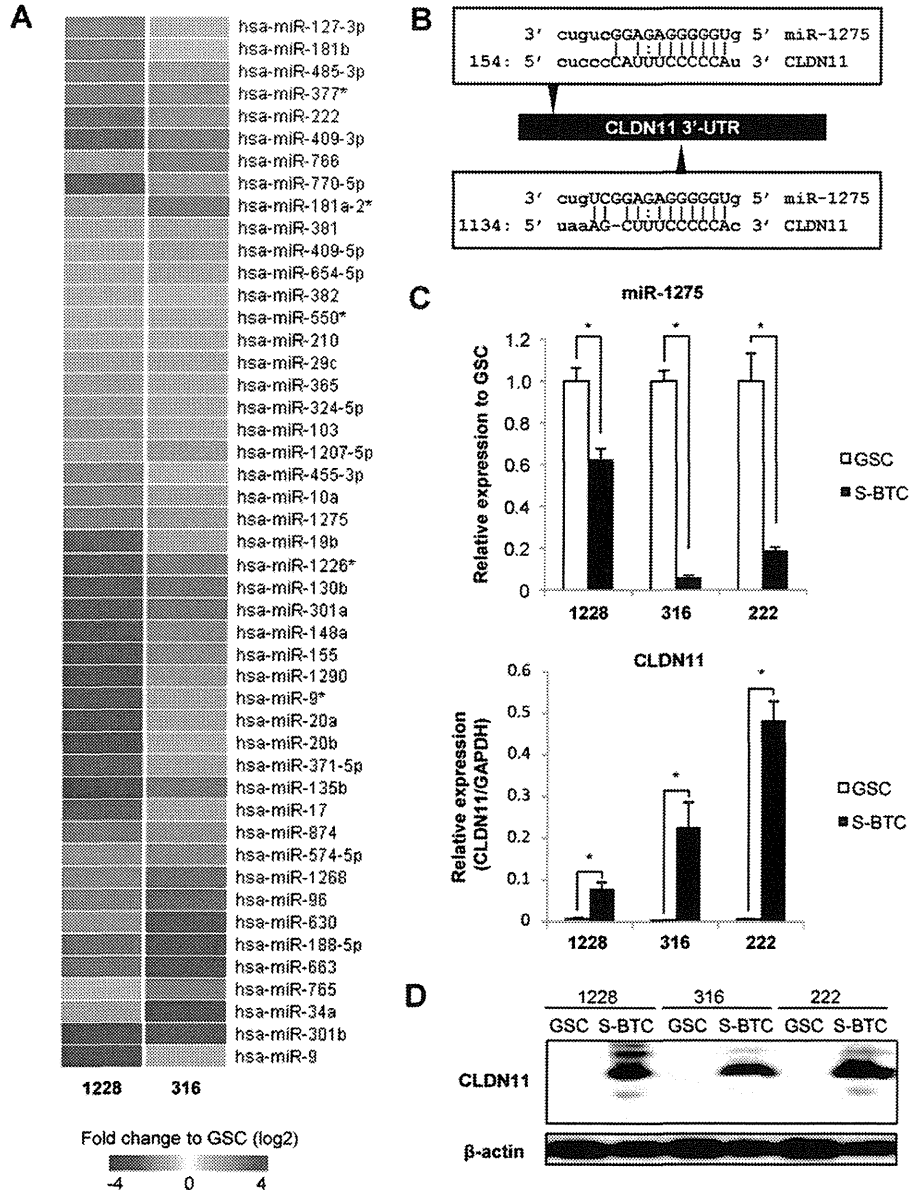

FIGURE 1. **miRNA microarray analysis in GSC lines.** *A*, heat map showing 13 miRNAs and 34 miRNAs that were commonly up-regulated (*red*) and down-regulated (*blue*) after serum exposure in two GSC lines (1228- and 316-GSCs). *hsa, Homo sapiens*. *B*, the predicted binding sites of miR-1275 are indicated (*arrowheads*) in the *CLDN11* 3′-UTR. Sequence alignments of miR-1275 with their corresponding potential binding sites in the *CLDN11* 3′-UTR are presented in each *rectangle*. Complementary sequence between *CLDN11* and miR-1275 are indicated above or beneath the *arrowheads*. Nucleotide positions of each target sites are indicated as relative to the position of the stop codon of *CLDN11* (The first nucleotide after the stop codon of *CLDN11* is defined as 1). *C*, qPCR analysis of miR-1275 expression in GSC and S-BTC (continuous serum exposure for 21 days). Expression levels were normalized to internal *RNU6B* control. Levels of miR-1275 expression in the three GSC cell lines were similar, and values are expressed relative to abundance of GSC (*upper panel*). *Lower panel*, qPCR analysis of *CLDN11* expression in GSC and S-BTC (continuous serum exposure for 21 days). Expression levels were normalized to internal *GAPDH* control. The assays were performed in three cell lines (1228-, 316-, and 222-GSCs), and the *error bars* indicate S.D. *, $p < 0.05$. *D*, Western blotting analysis of CLDN11 expression in GSC and S-BTC. β-Actin was used as a loading control.

luciferase activity in PC3 cells (supplemental Fig. 2*B*). Taken together, these results indicated that miR-1275 directly regulates *CLDN11* expression by targeting the two binding sites in the 3′-UTR of *CLDN11* mRNA.

miR-1275 Inhibits CLDN11 Protein Expression in GSC Cell Lines—To further assess the direct relationship between miR-1275 and *CLDN11* expression in GSCs, which showed a high level of miR-1275 and a low level of *CLDN11* mRNA expression, we examined the effects of anti-miR-1275 on CLDN11 expression in GSC cell lines. GSC lines were treated with anti-miR-1275, a negative control miRNA inhibitor (anti-N), or without any antisense molecules (mock control). In response to anti-miR-1275, mRNA expression of *CLDN11* was up-regulated along with the down-regulation of miR-1275 in three GSC lines (Fig. 3*A*). Consistently, both CLDN11 protein level and the number of CLDN11-positive cells were significantly increased in GSC spheroids after treatment with anti-miR-1275 in the three GSC lines (Fig. 3*B*).

We also found that GSCs treated with anti-miR-1275 showed significant growth suppression as compared with those treated with anti-N control, suggesting that inhibition of this miRNA could induce CLDN11 expression with rapid inhibition

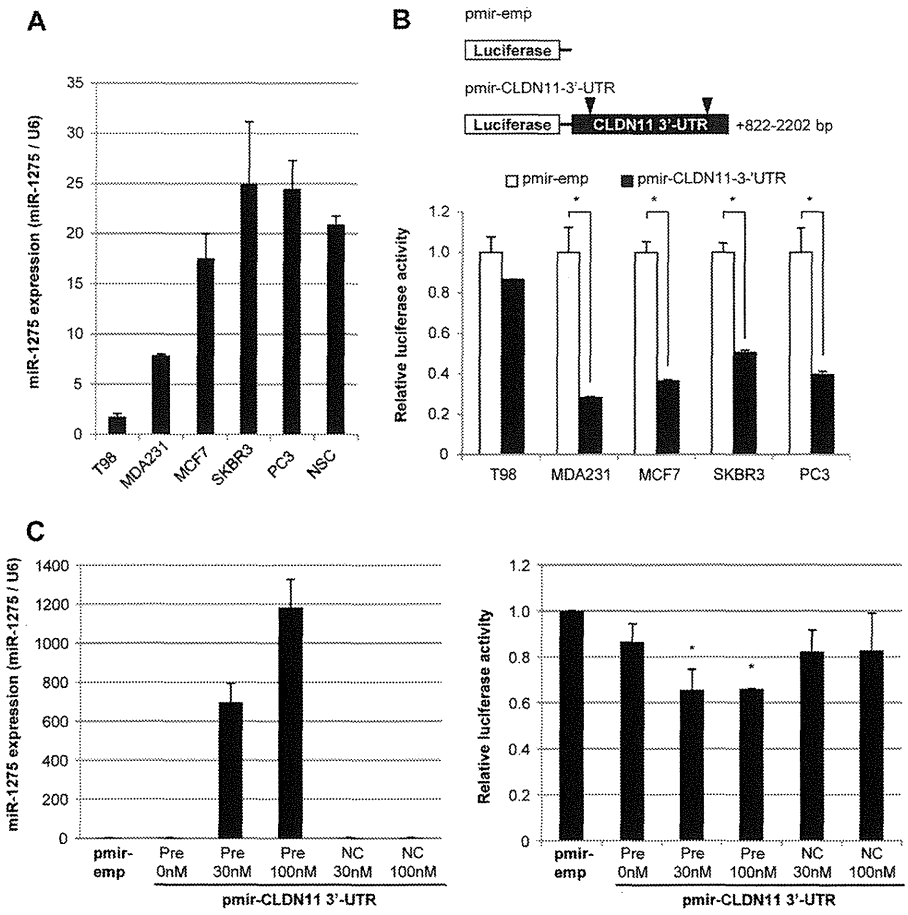

FIGURE 2. **Interaction between miR-1275 and its binding sites in the *CLDN11* 3′-UTR.** *A*, expression of miR-1275 in five human cancer cell lines (T98, MDA-MB-231, MCF7, SKBR3, and PC3) and human NSCs. Expression levels were normalized by *RNU6B* expression. *B*, Dual-Luciferase assay with pmir-CLDN11-3′-UTR reporter vector in cancer cell lines. Schemes of reporter vector with (*pmir-CLDN11 3′-UTR*) and without *CLDN11* 3′-UTR sequence (*pmir-emp*) are shown (*upper panel*). *Black triangles* indicate two miR-1275 binding sites within the 3′-UTR of the *CLDN11* gene. Luciferase values are indicated as relative to abundance of luciferase activity of pmir-emp (*bottom*). Assays were performed in triplicate. *Error bars* indicate S.D. *, $p < 0.05$. *C*, Dual-Luciferase assay with the pmir-CLDN11 3′-UTR reporter vector in T98 cells. Cells were co-transfected with 30 nM or 100 nM precursor molecules pre-miR-1275 (*Pre*) or negative control miRNA precursor (*NC*). Left, expression levels of miR-1275 are indicated. *Right*, values are indicated relative to abundance of luciferase activity of pmir-emp control. The assays were performed in triplicate. *Error bars* indicate S.D. *Asterisks* mean that repression of luciferase activity was significantly depressed in the indicated treatments as compared with pmir-emp control ($p < 0.05$).

of GSC proliferation (Fig. 3*C*). Further, we confirmed that inhibition of *CLDN11* by siRNA suppressed cell proliferation of GSCs (Fig. 3*D*).

miR-1275 Is Regulated by PRC2-mediated H3K27me3—Epigenetic control of developmental genes has emerged as a key mechanism for differentiation of NSCs in response to differentiation-inducing cues. Notably, a PRC2-H3K27me3-mediated gene silencing mechanism plays an essential part in the repression of key development-associated genes (36). To investigate whether this epigenetic mechanism is involved in the regulation of miR-1275, we examined the association between epigenetic status of the promoter region of pri-miR-1275 and miR-1275 expression in GSC lines. The transcriptional start site of pri-miR-1275 was determined by the DBTSS database (Fig. 4*A*) and confirmed by RT-PCR (supplemental Fig. 3) (37). Concordant with miR-1275 down-regulation during GSC differentiation into S-BTC, ChIP-PCR analysis showed that enrichment of H3K27me3 repressive mark and YY1 protein, together with loss of H3K9 acetylation (H3K9Ac) active mark in S-BTCs (Fig. 4*A*). Compellingly, treatment of GSCs with a potent PRC2 inhibitor, DZNep, showed sustained miR-1275 expression along with a small effect on *CLDN11* expression in the presence of serum (Fig. 4*B*, supplemental Fig. 4*A*). To clarify whether miR-1275 is regulated by an epigenetic pathway, especially PRC2-mediated mechanism, we further examined the effect of *EZH2*, a catalytic component of PRC2, inhibition on expression of miR-1275 and *CLDN11* using an shRNA system (*EZH2*-KD). *EZH2*-KD impaired serum-induced miR-1275 repression, resulting in disruption of *CLDN11* induction (supplemental Fig. 4*B*). These data suggested that induction of miR-1275 by differentiation-promoting serum conditions was responsible for increased expression of *CLDN11* via the PRC2-H3K27me3 epigenetic regulatory pathway.

Immunohistochemical Analysis of CLDN11 in Clinical Samples—To assess the impact of our findings in respect to the clinical features of glioblastoma, we investigated the expression pattern of CLDN11 in glioblastoma ($n = 3$) and normal brain ($n = 3$) tissues. CLDN11 was highly expressed in mature oligodendrocytes in normal brain (Fig. 5, *A* and *B*) (38). By contrast, in all three glioblastoma specimens, a major part of the tumor tissue was CLDN11-negative. Only one specimen showed a certain area composed of CLDN11-positive tumor cells (Fig. 5,

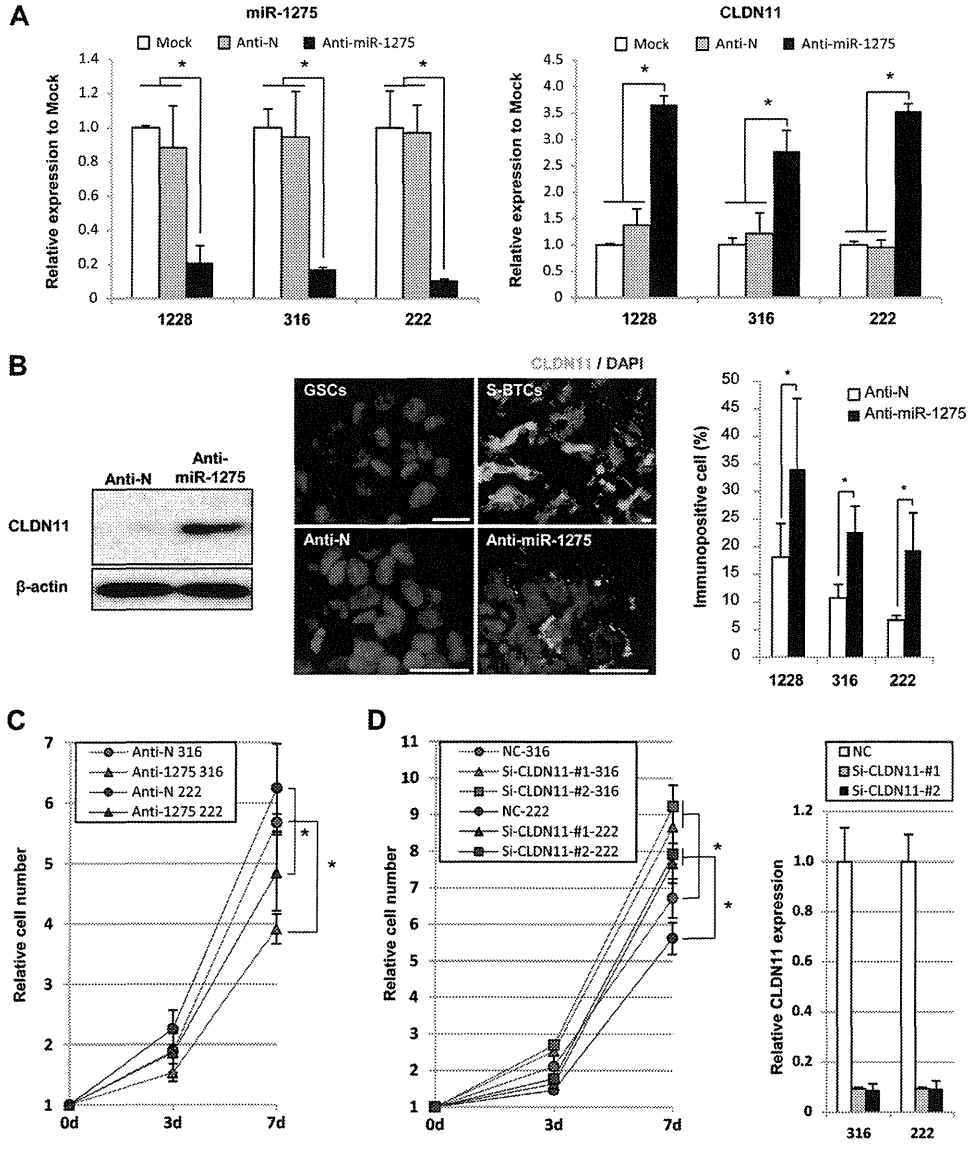

FIGURE 3. **miR-1275 targets *CLDN11* in GSCs.** *A*, expression levels of miR-1275 (*left*) and *CLDN11* (*right*) in three GSC lines are indicated. Cells were transfected with 100 nM anti-miR inhibitor against miR-1275 (*Anti-miR-1275*), a negative control miRNA inhibitor (*Anti-N*), or without any antisense molecules (*Mock*). Expression levels were normalized to internal *GAPDH* and *RNU6B* controls, respectively. Values are indicated relative to the levels of mock control. Assays were performed in triplicate. *Error bars* indicate S.D. *, $p < 0.05$. *B*, Western blot analysis of CLDN11 expression in GSC transfected with either 100 nM anti-miR-1275 or 100 nM anti-N. β-Actin was used as a loading control (*left panel*). Immunofluorescence analysis of CLDN11 in GSCs and S-BTCs was performed. GSCs were transfected with either 100 nM anti-miR-1275 or 100 nM anti-N (*middle*). *Bar*, 20 μm. The ratio of immunopositive cells in each sphere is shown (*right*). The *error bars* indicate S.D. *, $p < 0.01$. *C*, cell proliferation assay of GSC lines (316, 222) transfected with either 100 nM anti-miR-1275 (*triangle*) or 100 nM anti-N (*circle*). Values are expressed relative to abundance in 0 days. The *error bars* indicate S.D. *, $p < 0.05$. *D*, cell proliferation assay of GSC lines (316, 222) transfected with either 100 nM siRNA against *CLDN11* (*triangle*, siRNA-*CLDN11*, siRNA 1; *square*, siRNA 2) or 100 nM control siRNA (*NC*, *circle*) during GSC differentiation (*left*). Values are expressed relative to abundance at day 0. The *error bars* indicate S.D. *, $p < 0.05$. *CLDN11* mRNA expression levels (mean ± S.D.) in GSCs transfected with either siRNA-*CLDN11* or control siRNA are shown at the *right*.

C–E). To clarify whether these CLDN11-positive cells correspond to the oligodendroglial lineage, which sometimes present in a small fraction of glioblastomas (39, 40), we investigated the expression pattern of CLDN11 in comparison with major neural cell lineage markers, such as GFAP (an astrocyte lineage-specific marker), microtubule-associated protein 2 (MAP2, a neuron lineage-specific marker), and oligodendrocyte lineage transcription factor 2 (OLIG2, a oligodendrocyte lineage-specific marker). CLDN11-positive cells and GFAP-positive cells existed on a mutually exclusive basis in glioblastoma specimens. No MAP2-positive cells were found in the glioblastoma tissues examined. Notably, in small fractions of glioblastomas, CLDN11-positive cells were also positive for the anti-OLIG2 antibody, suggesting that CLDN11-positive cells in the glioblastoma tissues correspond to the oligodendroglial lineage and that regulation of miR-1275 may contribute, at least in part, to form the tissue heterogeneity corresponding to the oligodendroglial lineage cells in glioblastomas (Fig. 5, *F–I*).

DISCUSSION

Glioblastoma displays heterogeneous histological features, with subsets of tumor cells often showing distinct phenotypic states that differ in functional attributes. This phenotypic heterogeneity might be explained, at least in part, via a cancer

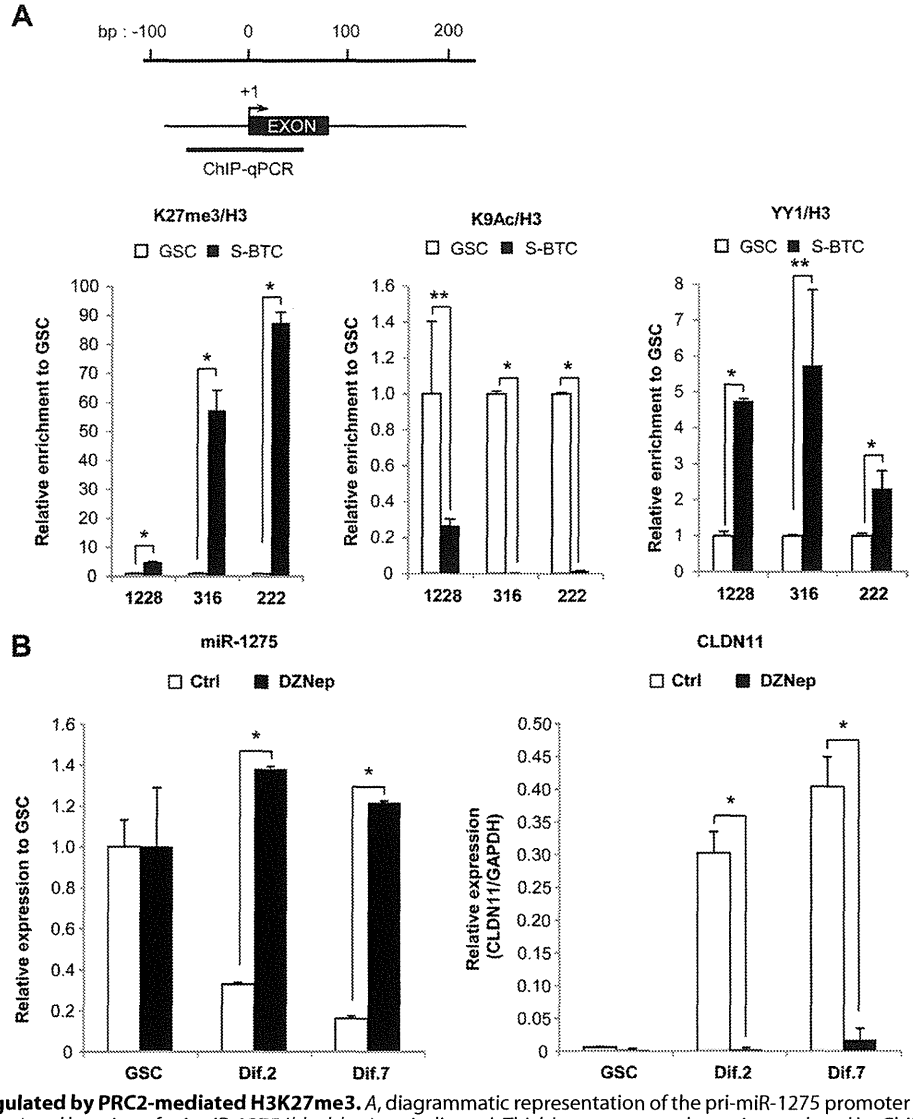

FIGURE 4. **miR-1275 is regulated by PRC2-mediated H3K27me3.** *A*, diagrammatic representation of the pri-miR-1275 promoter is shown (*upper panel*). The transcription start site (*arrow*) and location of pri-miR-1275 (*black box*) are indicated. *Thick bars* represent the region analyzed by ChIP-PCR. H3K27me3, H3K9Ac, and YY1 status in the pri-miR-1275 promoter region before (GSC, *white box*) and after serum exposure (S-BTC, *black box*) are shown (*lower panel*). Values are indicated relative to enrichment of each modification in GSCs. *Error bars* represent S.D. *, $p < 0.01$, **, $p < 0.05$. *B*, 222-GSCs were treated with DZNep (5 μM) followed by serum exposure. Expression levels of miR-1275 and *CLDN11* after continuous serum exposure for 2–7 days (*Dif.2* and *Dif.7*) with DZNep treatment are shown. The assays were performed in triplicate. *Error bars* indicate S.D. *, $p < 0.01$.

stem-like cell model (5). In this study, using a GSC-based differentiation model (4, 26, 27), we investigated the expression of miRNAs and associated epigenetic mechanisms that regulate the differentiation of GSCs. In response to serum-induced differentiation conditions, acquisition of H3K27me3 modification and enrichment of YY1 protein binding, which has been implicated to act as a modular scaffold protein to recruit PRC2 to the target genes (41, 42), together with loss of H3K9Ac in the pri-miR-1275 promoter region, led to the silencing of miR-1275 and derepression of its target, CLDN11, in GSCs. These findings support a model for the establishment of tissue heterogeneity where the tumor environment affects the expression of a subset of genes including miRNAs via plastic epigenetic mechanisms, resulting in distinct types of cell differentiation. We also examined DNA methylation status of a CpG island within the *CLDN11* promoter and found that no DNA methylation changes were detected in all three GSC lines, suggesting that this highly stable epigenetic machinery was not directly involved during GSC differentiation (supplemental Fig. 5). The significant difference between PRC2-H3K27me3 and DNA methylation centers on the stability of repression; indeed, H3K27me3-mediated gene silencing can change dynamically during differentiation, as opposed to DNA methylation within CpG islands, which is highly stable and irreversible without artificially altering key factors in cells (43).

The most prevalent form of glioma is referred to as astrocytoma. However, glioblastoma also contains an oligodendrocyte component in some cases. This oligodendroglial component has been detected in ~20% of glioblastomas; moreover, the presence of oligodendroglial components has been reported to be predictive of longer survival of patients in certain studies (39, 40). Our immunohistochemical examination revealed that CLDN11-positive tumor cells also showed OLIG2 positivity in a specific region of tumors, with this area being in concordance with an oligodendroglial component; this suggests that CLDN11 expression via down-regulation of miR-1275 contrib-

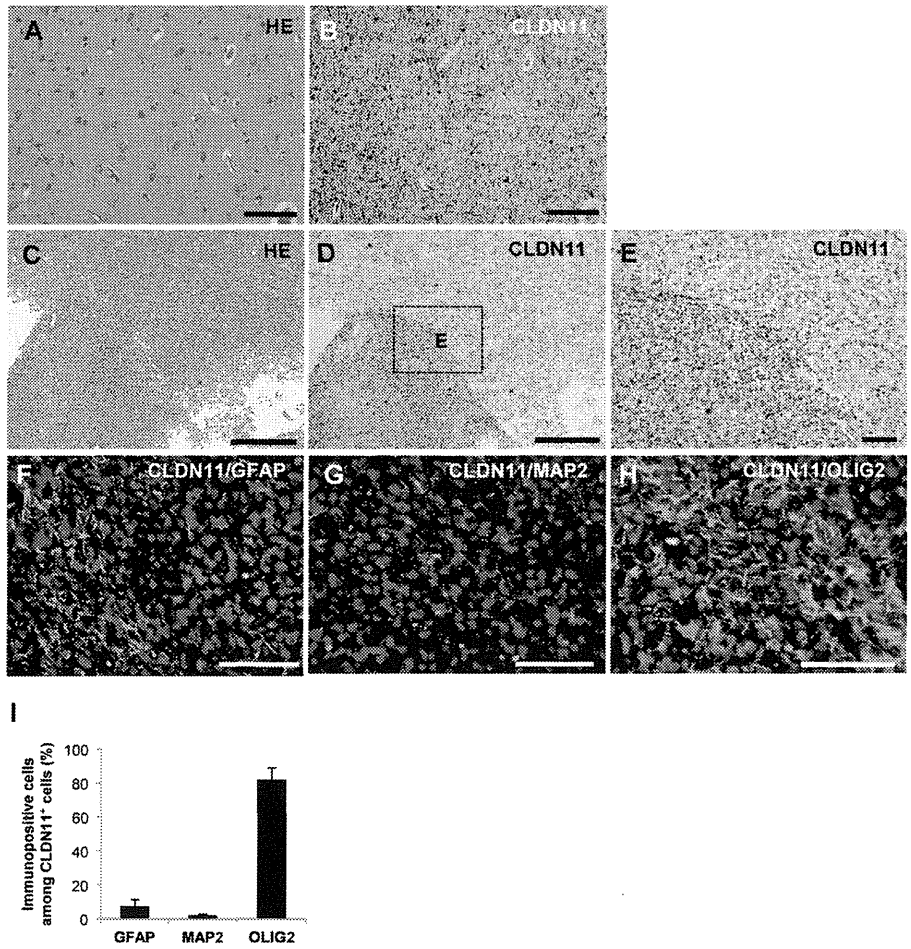

FIGURE 5. **Immunohistochemistry of CLDN11 and neural lineage-specific marker in clinical samples.** *A* and *B*, hematoxylin/eosin (*HE*) staining (*A*) and corresponding immunohistochemistry of CLDN11 in normal brain (white matter) (*B*). *Bar*, 100 μm. *C* and *D*, hematoxylin/eosin staining of glioblastoma section (*C*) and corresponding immunohistochemical analysis of CLDN11 in glioblastoma section (*D*). *Bar*, 500 μm. *E*, the area in *panel D* is magnified. *Bar*, 100 μm. *F–H*, immunofluorescence analysis of CLDN11 (*green*) and GFAP (*red*) (*F*), CLDN11 (*green*), and MAP2 (*red*) (*G*), and CLDN11 (*green*) and OLIG2 (*red*) (*H*) in glioblastoma. Cells are also stained with DAPI to highlight nuclear areas. *Bar*, 100 μm. *I*, ratio of immunopositive cells to each neural-lineage marker among CLDN11-positive cells is counted. *Error bars* indicate S.D.

utes to the formation of oligodendroglial component in glioblastoma.

We noted that GSC with ectopic expression of miR-1275 could convert into S-BTC with *GFAP* and *Tuj1* positives under differentiation-promoting serum conditions (supplemental Fig. 6). This suggests that miR-1275 particularly affected the expression of CLDN11, which is an important protein for oligodendroglial lineage differentiation but is not a master regulator of the other differentiation-associated genes in GSCs.

Although miR-205 has been reported as a potential regulator of CLDN11 in human embryonic stem cell differentiation, this miRNA did not appear to be involved in GSC differentiation into oligodendroglial lineage in our model (35). Another miRNA, miR-219, has been shown to be necessary and sufficient to promote oligodendrocyte differentiation (44). However, expression of this miRNA was also at an undetectable level in our microarray analysis of the three GSC cell types (ArrayExpress, accession codes: GSE36201). In addition to GSCs, we also found that miR-1275 may affect the expression of CLDN11 during NSC differentiation mediated by retinoic acid exposure. Because miRNAs are potential key regulators of differentiation and miRNA-deficient mice with Dicer deletions showed significant impairment of oligodendrocyte differentiation and production of myelin genes (44, 45), miR-1275 might also be one of the key miRNAs for myelination and oligodendroglial lineage differentiation.

Recent studies indicate that miRNAs are essential regulators of GSCs. miR-9/9* is highly abundant in CD133+ cells, and inhibition of miR-9/9* leads to reduced neurosphere formation (13). Members of the miR-17–92 cluster are down-regulated upon GSC differentiation. Transfection of inhibitors of the miR-17–92 cluster induced increased apoptosis and decreased cell proliferation (15). Consistent with these previous studies, down-regulation of miR-9/9* and miR-17, miR-19b, and miR-20a, components of the miR-17–92 cluster, were detected during GSC differentiation in our microarray analysis. In addition to these findings, we found that suppression of miR-1275 in GSCs induced oligodendroglial lineage-associated protein (CLDN11) along with rapid inhibition of GSC proliferation.

The loss of tumor-suppressive miRNAs enhances the expression of target oncogenes, whereas increased expression of oncogenic miRNAs (known as oncomirs) can repress tumor-suppressor genes in cancers (46). Members of the Claudin gene family are expressed in both a tissue stage-specific and a devel-

opmental stage-specific manner. CLDN11 expression is highly regulated during development and may play an important role in growth and differentiation of oligodendrocytes. In cancer cells, CLDN11 appears to have a tumor-suppressor function in gastric cancer, bladder cancer, and meningioma (47–49). Indeed, inhibition of CLDN11 by siRNA in GSCs induced cell proliferation (Fig. 3*D*). Given these tumor-suppressor functions of CLDN11, miR-1275 may also have a context-dependent effect; in cancer cells (including our GSCs), it works as an oncomir, inhibition of which may also lead the suppression of tumor cell growth. This is also explained by the ideas that developmentally important genes also have crucial roles during tumor progression in a lineage-specific context (50).

In summary, our data provide evidence that repression of miR-1275 via PRC2-H3K27me3 results in CLDN11 up-regulation, which may be required for the tumor cell differentiation and contribute to the establishment of tissue heterogeneity in glioblastoma. In addition, miR-1275 targets CLDN11, which represses the proliferation of tumor cells, as was found in the current study. These results have illuminated the epigenetic regulatory pathways for tumor cell differentiation by miR-1275 in glioblastomas, inhibition of which may be a potential target for cancer therapy as a new clinical application.

Acknowledgments—We thank Ms. Ikuko Tomimatsu for her experimental assistance. NSC was a kind gift from Dr. Seung U. Kim at Medical Research Institute, Chung-Ang University College of Medicine.

REFERENCES

1. Bonavia, R., Inda, M. M., Cavenee, W. K., and Furnari, F. B. (2011) Heterogeneity maintenance in glioblastoma: a social network. *Cancer Res.* **71,** 4055–4060
2. Phillips, H. S., Kharbanda, S., Chen, R., Forrest, W. F., Soriano, R. H., Wu, T. D., Misra, A., Nigro, J. M., Colman, H., Soroceanu, L., Williams, P. M., Modrusan, Z., Feuerstein, B. G., and Aldape, K. (2006) Molecular subclasses of high-grade glioma predict prognosis, delineate a pattern of disease progression, and resemble stages in neurogenesis. *Cancer Cell* **9,** 157–173
3. Singh, S. K., Hawkins, C., Clarke, I. D., Squire, J. A., Bayani, J., Hide, T., Henkelman, R. M., Cusimano, M. D., and Dirks, P. B. (2004) Identification of human brain tumor initiating cells. *Nature* **432,** 396–401
4. Lee, J., Kotliarova, S., Kotliarov, Y., Li, A., Su, Q., Donin, N. M., Pastorino, S., Purow, B. W., Christopher, N., Zhang, W., Park, J. K., and Fine, H. A. (2006) Tumor stem cells derived from glioblastomas cultured in bFGF and EGF more closely mirror the phenotype and genotype of primary tumors than do serum-cultured cell lines. *Cancer Cell* **9,** 391–403
5. Gupta, P. B., Chaffer, C. L., and Weinberg, R. A. (2009) Cancer stem cells: mirage or reality? *Nat. Med.* **15,** 1010–1012
6. Gupta, P. B., Fillmore, C. M., Jiang, G., Shapira, S. D., Tao, K., Kuperwasser, C., and Lander, E. S. (2011) Stochastic state transitions give rise to phenotypic equilibrium in populations of cancer cells. *Cell* **146,** 633–644
7. Cho, R. W., Wang, X., Diehn, M., Shedden, K., Chen, G. Y., Sherlock, G., Gurney, A., Lewicki, J., and Clarke, M. F. (2008) Isolation and molecular characterization of cancer stem cells in MMTV-Wnt-1 murine breast tumors. *Stem Cells* **26,** 364–371
8. Deshpande, A. J., Cusan, M., Rawat, V. P., Reuter, H., Krause, A., Pott, C., Quintanilla-Martinez, L., Kakadia, P., Kuchenbauer, F., Ahmed, F., Delabesse, E., Hahn, M., Lichter, P., Kneba, M., Hiddemann, W., Macintyre, E., Mecucci, C., Ludwig, W. D., Humphries, R. K., Bohlander, S. K., Feuring-Buske, M., and Buske, C. (2006) Acute myeloid leukemia is propagated by a leukemic stem cell with lymphoid characteristics in a mouse model of CALM/AF10-positive leukemia. *Cancer Cell* **10,** 363–374
9. Wu, A., Oh, S., Wiesner, S. M., Ericson, K., Chen, L., Hall, W. A., Champoux, P. E., Low, W. C., and Ohlfest, J. R. (2008) Persistence of $CD133^+$ cells in human and mouse glioma cell lines: detailed characterization of GL261 glioma cells with cancer stem cell-like properties. *Stem Cells Dev.* **17,** 173–184
10. Bartel, D. P. (2004) MicroRNAs: genomics, biogenesis, mechanism, and function. *Cell* **116,** 281–297
11. Gangaraju, V. K., and Lin, H. (2009) MicroRNAs: key regulators of stem cells. *Nat. Rev. Mol. Cell Biol.* **10,** 116–125
12. Medina, P. P., and Slack, F. J. (2008) MicroRNAs and cancer: an overview. *Cell Cycle* **7,** 2485–2492
13. Schraivogel, D., Weinmann, L., Beier, D., Tabatabai, G., Eichner, A., Zhu, J. Y., Anton, M., Sixt, M., Weller, M., Beier, C. P., and Meister, G. (2011) CAMTA1 is a novel tumour suppressor regulated by miR-9/9* in glioblastoma stem cells. *EMBO J.* **30,** 4309–4322
14. Chan, J. A., Krichevsky, A. M., and Kosik, K. S. (2005) MicroRNA-21 is an antiapoptotic factor in human glioblastoma cells. *Cancer Res.* **65,** 6029–6033
15. Ernst, A., Campos, B., Meier, J., Devens, F., Liesenberg, F., Wolter, M., Reifenberger, G., Herold-Mende, C., Lichter, P., and Radlwimmer, B. (2010) Derepression of CTGF via the miR-17–92 cluster upon differentiation of human glioblastoma spheroid cultures. *Oncogene* **29,** 3411–3422
16. Gillies, J. K., and Lorimer, I. A. (2007) Regulation of $p27^{Kip1}$ by miRNA 221/222 in glioblastoma. *Cell Cycle* **6,** 2005–2009
17. Jones, P. A., and Baylin, S. B. (2002) The fundamental role of epigenetic events in cancer. *Nat. Rev. Genet.* **3,** 415–428
18. Bracken, A. P., and Helin, K. (2009) Polycomb group proteins: navigators of lineage pathways led astray in cancer. *Nat. Rev. Cancer* **9,** 773–784
19. Noushmehr, H., Weisenberger, D. J., Diefes, K., Phillips, H. S., Pujara, K., Berman, B. P., Pan, F., Pelloski, C. E., Sulman, E. P., Bhat, K. P., Verhaak, R. G., Hoadley, K. A., Hayes, D. N., Perou, C. M., Schmidt, H. K., Ding, L., Wilson, R. K., Van Den Berg, D., Shen, H., Bengtsson, H., Neuvial, P., Cope, L. M., Buckley, J., Herman, J. G., Baylin, S. B., Laird, P. W., and Aldape, K. (2010) Identification of a CpG island methylator phenotype that defines a distinct subgroup of glioma. *Cancer Cell* **17,** 510–522
20. Saito, Y., Liang, G., Egger, G., Friedman, J. M., Chuang, J. C., Coetzee, G. A., and Jones, P. A. (2006) Specific activation of microRNA-127 with down-regulation of the proto-oncogene BCL6 by chromatin-modifying drugs in human cancer cells. *Cancer Cell* **9,** 435–443
21. Cao, Q., Mani, R. S., Ateeq, B., Dhanasekaran, S. M., Asangani, I. A., Prensner, J. R., Kim, J. H., Brenner, J. C., Jing, X., Cao, X., Wang, R., Li, Y., Dahiya, A., Wang, L., Pandhi, M., Lonigro, R. J., Wu, Y. M., Tomlins, S. A., Palanisamy, N., Qin, Z., Yu, J., Maher, C. A., Varambally, S., and Chinnaiyan, A. M. (2011) Coordinated regulation of polycomb group complexes through microRNAs in cancer. *Cancer Cell* **20,** 187–199
22. Polyak, K., and Weinberg, R. A. (2009) Transitions between epithelial and mesenchymal states: acquisition of malignant and stem cell traits. *Nat. Rev. Cancer* **9,** 265–273
23. Nottke, A., Colaiácovo, M. P., and Shi, Y. (2009) Developmental roles of the histone lysine demethylases. *Development* **136,** 879–889
24. Shen, X., Liu, Y., Hsu, Y. J., Fujiwara, Y., Kim, J., Mao, X., Yuan, G. C., and Orkin, S. H. (2008) EZH1 mediates methylation on histone H3 lysine 27 and complements EZH2 in maintaining stem cell identity and executing pluripotency. *Mol. Cell* **32,** 491–502
25. Mohn, F., and Schübeler, D. (2009) Genetics and epigenetics: stability and plasticity during cellular differentiation. *Trends Genet.* **25,** 129–136
26. Yuki, K., Natsume, A., Yokoyama, H., Kondo, Y., Ohno, M., Kato, T., Chansakul, P., Ito, M., Kim, S. U., and Wakabayashi, T. (2009) Induction of oligodendrogenesis in glioblastoma-initiating cells by IFN-mediated activation of STAT3 signaling. *Cancer Lett.* **284,** 71–79
27. Natsume, A., Kato, T., Kinjo, S., Enomoto, A., Toda, H., Shimato, S., Ohka, F., Motomura, K., Kondo, Y., Miyata, T., Takahashi, M., and Wakabayashi, T. (2012) Girdin maintains the stemness of glioblastoma stem cells. *Oncogene* **31,** 2715–2724
28. Kim, S. U. (2004) Human neural stem cells genetically modified for brain repair in neurological disorders. *Neuropathology* **24,** 159–171
29. Kondo, Y., Shen, L., Cheng, A. S., Ahmed, S., Boumber, Y., Charo, C.,